The sounds of a helicopter on Mars

Ralph D Lorenz, Sylvestre Maurice, Baptiste Chide, David Mimoun, Alexander Stott, Naomi Murdoch, Martin Giller, Xavier Jacob, Roger C Wiens, Franck Montmessin, et al.

Planetary and Space Science 230 (2023) 105684

Contents lists available at ScienceDirect

Planetary and Space Science

journal homepage: www.elsevier.com/locate/pss

The sounds of a helicopter on Mars

Ralph D. Lorenz [a,*], Sylvestre Maurice [b], Baptiste Chide [c], David Mimoun [d], Alexander Stott [d], Naomi Murdoch [d], Martin Giller [d], Xavier Jacob [e], Roger C. Wiens [f], Franck Montmessin [g], Håvard Grip [h], Theodore Tzanetos [h], Bob Balaram [h], Nathan Williams [h], Matt Keennon [i], Sara Langberg [i], Jeremy Tyler [i], Tanguy Bertrand [j], Adrian Brown [k], Nicolas Randazzo [l], Benjamin Pipenberg [m]

[a] Johns Hopkins Applied Physics Laboratory, 11100 Johns Hopkins Road, Laurel, MD, 20723, USA
[b] Institut de Recherche en Astrophysique et Planétologie, Université de Toulouse 3 Paul Sabatier, CNRS, CNES, Toulouse, France
[c] Space and Planetary Exploration Team, Los Alamos National Laboratory, Los Alamos, NM, USA
[d] Institut Supérieur de l'Aéronautique et de l'Espace (ISAE-SUPAERO), Université de Toulouse, Toulouse, France
[e] Institut de Mécanique des Fluides de Toulouse, Univ. Toulouse 3 Paul Sabatier, INP, CNRS, Toulouse, France
[f] Earth, Atmospheric, and Planetary Sciences, Purdue University, West Lafayette, IN, 47907, USA
[g] Laboratoire Atmosphères, Milieux, Observations Spatiales, CNRS, Univ. Saint-Quentin-en-Yvelines, Sorbonne Univ., Guyancourt, France
[h] Jet Propulsion Laboratory, California Institute of Technology, 4800 Oak Grove Drive, Pasadena, CA, 91109, USA
[i] Aerovironment, Inc., Simi Valley, CA, USA
[j] LESIA, Observatoire de Paris, 92195 Meudon, France
[k] Plancius Research, Severna Park, MD, 21146, USA
[l] Department of Earth and Atmospheric Sciences, University of Alberta, Canada
[m] Knightwerx, Simi Valley, CA, USA

ARTICLE INFO

Handling Editor: Dr Olivier Witasse

ABSTRACT

The sounds of the Ingenuity Helicopter flying in the Martian atmosphere are among the most notable recordings of the microphone on the SuperCam instrument on the Mars 2020 Perseverance Rover. Distinct acoustic signatures of the helicopter were recorded on the 4th, 5th, 6th, and 8th flights: prior to this, simultaneous microphone and helicopter operations had not been verified in the testbed, and generally since these early flights the helicopter has been too far away for its emissions to be detectable given CO_2 absorption in the Mars atmosphere.

The detected signatures are around 84 Hz and (occasionally) at 168 Hz, at the blade crossing frequency and its first harmonic. Several higher harmonics were prominent in hover tests in short-range recordings in a test chamber on Earth; these are attenuated by CO_2 absorption at the 50m-plus ranges on Mars. Doppler shift of the 84 Hz signal can be measured and is consistent with the trajectory measured with Ingenuity's navigation camera and inertial navigation unit, and documented by Perseverance's cameras.

A striking feature of the sound recordings is an unanticipated deep modulation of the signals with nulls spaced by around 15–20s, superposed on the simple and expected decline in amplitude with distance. We have evaluated and rejected models of multipath sound interference as requiring implausibly strong near-surface temperature gradients. We find instead that the modulation appears to be the signature of a slight asynchrony between the rotation rates of the two coaxial rotors, such that the blade-crossing azimuth rotates slowly during flight, resulting in a 'lighthouse' sweeping of the radiated sound pattern. Analysis of blade orientations seen in the shadow of the helicopter observed in down-looking navigation images supports this model.

1. Introduction

The Mars 2020 Perseverance rover is the first Mars mission that has been able to return acoustic data in the audible range (i.e. 20 Hz to 20 kHz) from the surface, notably from a microphone that is part of the SuperCam instrument (Maurice et al., 2022). Among the sounds recorded are wind and turbulence noise and various equipment operations. Most prominent among these is the sound of the Ingenuity helicopter. This paper

* Corresponding author.
E-mail address: RALPH.LORENZ@JHUAPL.EDU (R.D. Lorenz).

https://doi.org/10.1016/j.pss.2023.105684
Received 16 December 2022; Received in revised form 29 March 2023; Accepted 1 April 2023
Available online 6 April 2023

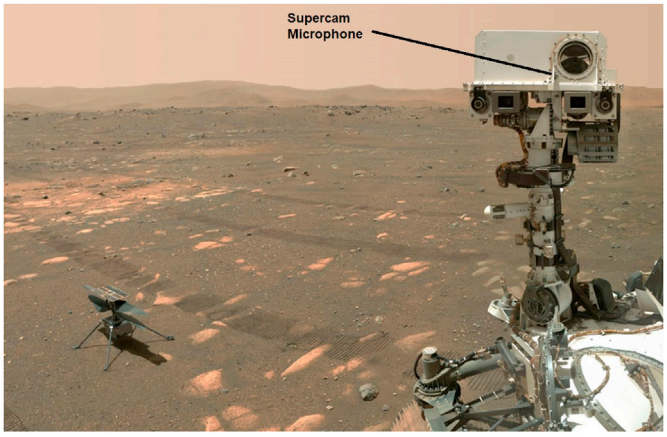

Fig. 1. The Ingenuity helicopter on Mars shortly after its deployment, observed at left in a mosaic of some 62 individual images acquired using an arm-mounted camera (WATSON) on April 6, 2021 (Sol 46). The mosaic also shows the remote sensing mast at the right, including the Supercam mast unit and its microphone. NASA/JPL-Caltech/Malin Space Science Systems.

documents the acoustic features of helicopter flights and their relation to flight parameters and ambient conditions. Because the source characteristics are somewhat known, the sounds are of potential interest as a probe of the near-surface atmosphere (e.g. Ingård, 1953; Piercy et al., 1977).

Ingenuity (Fig. 1) is a 1.8 kg coaxial helicopter with two-bladed rotors that spin at nominally 2537 rpm (see e.g. Balaram et al., 2018; Lorenz, 2022 and Tzanetos et al., 2022; the rotors were operated at a higher speed in some later flights when atmospheric density was lower). At the time of writing[1] (600 Sols into the Perseverance mission: a Martian solar day or Sol is 24.7 Earth days long), the helicopter has made some 33 flights on Mars, although its technology demonstration objectives required only 5 flights (performed between Sols 58 and 76), documented by the helicopter's own telemetry and imaging, as well as in movies by the Mastcam-Z instrument on the rover. After the initial objectives were met, progressively more ambitious flights were made, achieving longer flight ranges – see, for example, Grip et al. (2022) – and imaging from the helicopter viewed the terrain at Jezero beyond the view of Perseverance's cameras, as well as documenting the disposition of the mission's entry and descent hardware. Additionally, downwash from the rotors during proximity to the ground caused faint dust clouds to be formed (Lemmon et al., 2022), yielding some insights into Aeolian interactions in the Martian surface environment.

Safety considerations (the rover hardware must be protected to execute its sample caching function) meant that the helicopter has so far not been permitted to operate closer to the rover than about 50m distance. Additionally, the simultaneous operation of the Supercam instrument with the helicopter base station had to be verified to be safe before microphone observations could be made. Thus, it was only on the 4th flight that acoustic recordings were first attempted, and most of the flights since have been at distances too far for acoustic emissions from the helicopter to be detectable. However, the acoustic signature of the helicopter has been recorded on four flights (4,5,6, and 8), permitting a robust characterization of the emission and propagation of the sound from this unique vehicle.

2. Acoustic data and helicopter flight operations

The sound recordings were performed by the microphone on the Supercam instrument (Maurice et al., 2021; Mimoun et al., 2023; Chide et al., 2023), mounted on the Perseverance rover's Remote Sensing Mast (RSM). The RSM unit was aimed at the helicopter, principally to document the flights with the Mastcam-Z instrument, and in most cases, the rover was oriented so that the heli base station radio antenna was in direct line of sight to Ingenuity.

The microphone recorded at 25 kilosamples per second (e.g. Maurice et al., 2022), and the sound record (limited by a data buffer) is 167 s long, fortunately long enough to capture the entirety of the flights. Both the helicopter flight and the Supercam sound recording, were triggered by time-tagged commands – there was no synchronization communication between Ingenuity and Perseverance.

A summary of the relevant flight characteristics is given in Table 1: additional data, including the start/end location referenced to a standard Jezero map projection, are provided in Appendix 1. The helicopter coordinates were derived by registering helicopter navigation camera mosaics to an orbital HiRISE basemap. The geometry of the flights is illustrated in Figs. 2–5.

An important additional dataset for interpreting the acoustic data is the helicopter navigation camera images. The down-looking greyscale images are used in real-time on board the helicopter where successive images are cross-correlated to derive the velocity over the ground. A subset of these images is downlinked via the rover to the ground after the flight. These images can be mosaicked and a rather precise position history derived. The entire groundtrack of flight 5 was documented by ortho-mosaiced navigation camera images, but only a small selection of images, covering small parts of the outbound leg of flight 4, and part of flight 6, were returned on those flights. Since the flights were performed near noon (typically 12:33 Local Mean Solar Time, 12:33 LMST, a time

Table 1
Characteristics of acoustically-observed flights.

Flight	Sol	Flight Plan	Activities
4	69	Hover, move southward 133 m, hover, return, hover, land back at Wright Brothers Field	Took color images while hovering at its farthest point from takeoff. Horizontal flight at 3.5 m/s.
5	76	Hover, shift southwards 129 m, climb to 10 m, hover, land at Airfield B	This was the first flight to land at a new location 129 m south. On arrival, it gained altitude, hovered, captured a few color terrain images and then landed at that new site, Airfield B. Horizontal flight at 2 m/s and vertical flight at 1 m/s.
6	91	Translate southwest about 150 m, southward about 15 m, northeast about 50 m, land near Airfield C	This flight was the first in the operation demonstration phase. Towards the end of the first leg of the route a glitch in the navigation image processing system led to jerking control.*Ingenuity* landed about 5 m away from the planned site, assumed as its Airfield C, at the time only previously observed in orbital imagery
8	120	Translate south south-east 160 m to land at Airfield E	Takeoff point was 65m from Perseverance: the landing spot was about 135 m distant.
9	133	Translate 600m Southwest to Airfield F	Long flight over Séítah sand dunes. Takeoff was 200m from rover, landing was some 516m away.

Note that a guidance anomaly occurred on flight 6, where 54 s after takeoff the load on the onboard computer associated with transferring an image from the color Return To Earth (RTE) camera led to the dropping of a navigation camera frame. Subsequent navigation camera frames then arrived with an incorrect time tag, resulting in attitude solution errors which caused the helicopter to buck violently due to attempts to correct these 'phantom' errors. It is tempting to speculate that these gyrations might have been detectable in the sound recording, but unfortunately, this anomaly occurred in a part of the flight that was too distant from the rover for the helicopter to be audible. Investigation and resolution of this anomaly substantially influenced the planning and execution of subsequent flights. In addition to telemetry from the helicopter guidance system (not presently publicly-available) some of the helicopter flights were documented by imaging from the rover – see e.g. Bell et al. (2022) and Lemmon et al. (2022).

[1] Revisions to this paper were made around Sol 720, when a total of some 45 helicopter flights had been made. The helicopter remains too distant to hear, however.

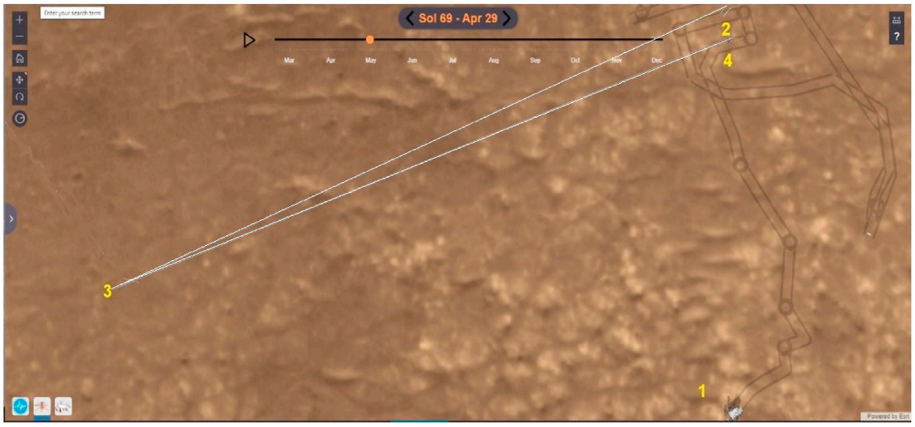

Fig. 2. Synthetic view from overhead, using HiRISE basemap, of Flight 4. The rover is shown at position 1; the helicopter took off from Wright Brothers Field (2) and flew to the south (3) before returning to near its takeoff point (4). Thus the flight path was largely orthogonal to the direction of the rover (closest approach ~72m) and subtended about 120 degrees of azimuth. Note the rover tracks near sites 2 & 4: these are visible in navigation camera images (see Fig. 14). Visualization software is the Rice University Mars 2020 Mission Tracker at https://www.perseverancerover.spatialstudieslab.org/.

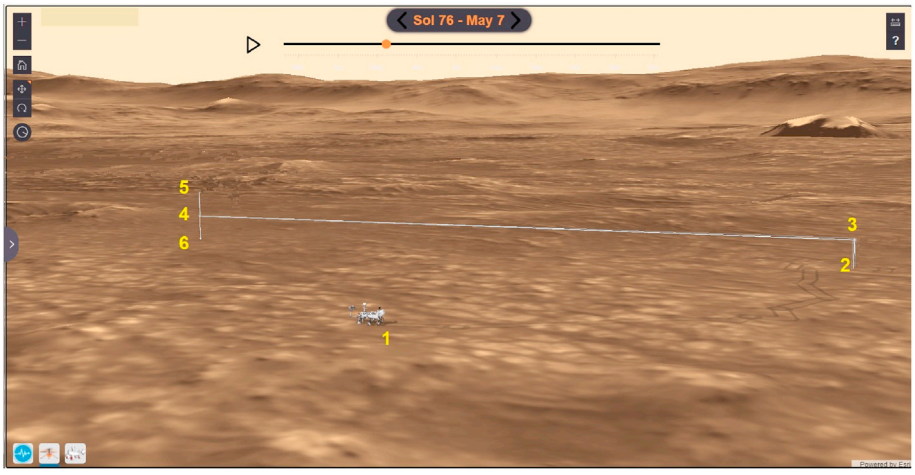

Fig. 3. A synthetic view of Jezero crater using orbital images draped on a digital terrain model showing Helicopter flight 5 seen from behind the rover (1). (The rover position is almost the same as in Fig. 2, and the flight path is almost perfectly superposed on that of flight 4, seen from overhead in the previous figure). Here the helicopter takes off (2) climbing to 5m (3), then translates horizontally to the south by about 130m to (4), where it stops, climbs to 10m (5) and hovers, then descends to land at (6). Author annotations on visualization generated per Fig. 2.

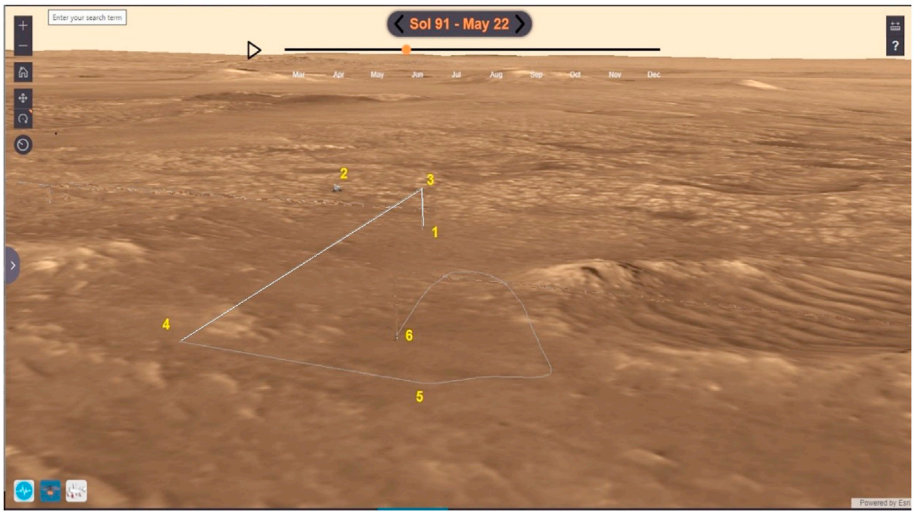

Fig. 4. Synthetic view of flight 6, looking back from beyond the landing site back towards the takeoff point(1) and the rover (2). The flight path was initially to the west almost radially (3–4) away from the rover, then made a right-angle turn to the left before the flight path became irregular (5) before a safe landing (6). Only the (well-controlled) takeoff and outbound straight segments in white were observable acoustically, the southbound leg (4–5) and irregular (5–6) segments in grey were too far to be heard. Figure generation as Figs. 2 and 3.

chosen as a compromise among battery state of charge, helicopter temperatures, atmospheric density and wind, and gustiness conditions), the downlooking images show the shadow of the helicopter, which turns out to be important as we discuss in a later section. Atmospheric conditions during the helicopter flights are reported in Viúdez-Moreiras et al. (2022): mean wind speeds were 4.3 and 3.3 m/s during flights 4 and 6, while rather higher (mean 6.4 m/s) during flight 8. Wind data were not reported on flights 5 or 9. A more general description of meteorological conditions at Jezero is given by Newman et al. (2022).

3. Acoustic observations

3.1. Overall characteristics

The spectrograms, time series and averaged spectra of the four flights documented acoustically are shown in Figs. 6-9: the spectrograms were generated by Fourier transforming 2-s windows of data, tapered with a Hanning window, and overlapping by 1s. These data have been filtered to remove a continuous rover-induced noise at 195 Hz (attributed to the

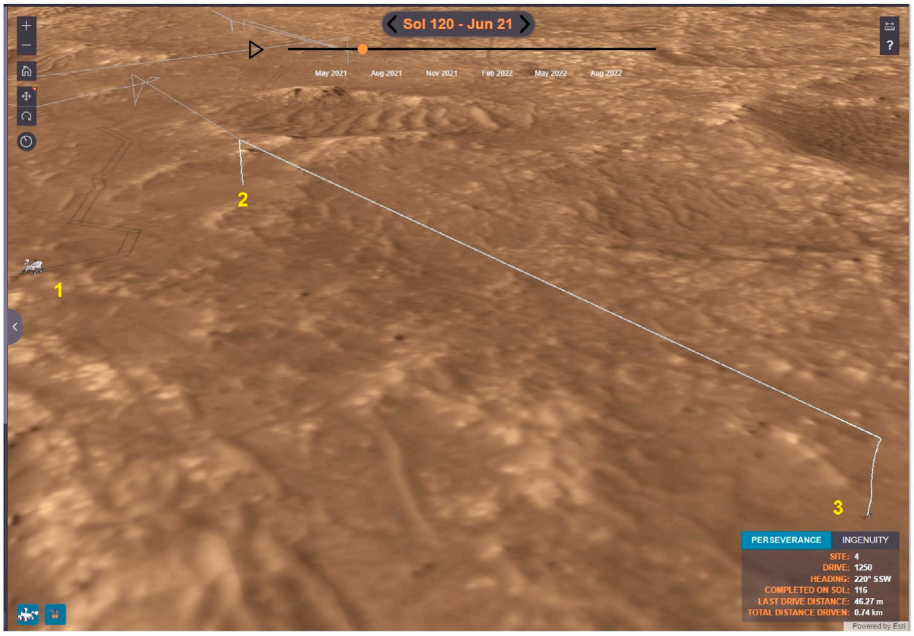

Fig. 5. Synthetic view of flight 8, looking North from over Seitah. The rover is shown (1), relatively near the takeoff point (2). The flight path was southwest at 10m altitude to land at (3). Some of the previous flight paths are visible in grey at the upper left. View generated as Fig. 2.

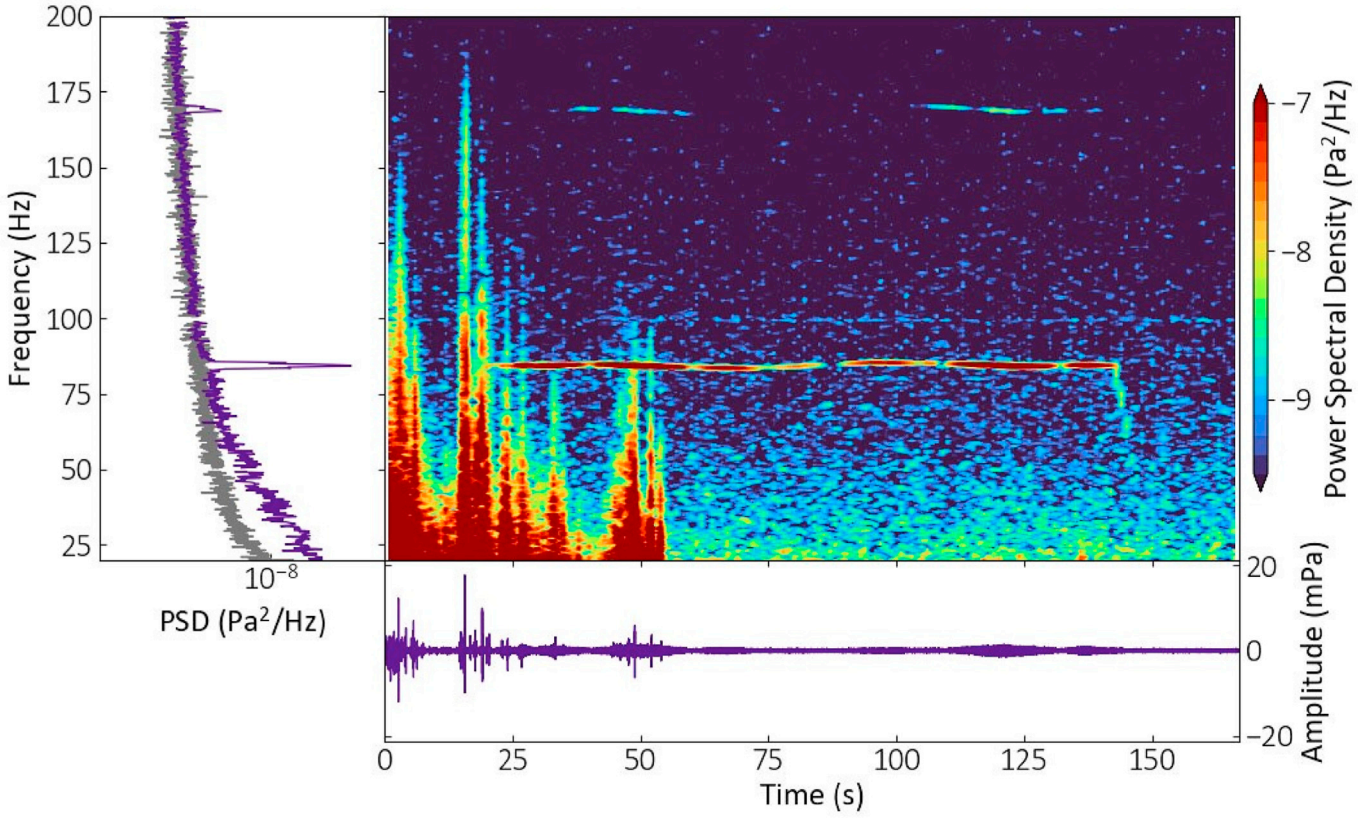

Fig. 6. The first flight with sound recording (Flight #4) had the spin-up and takeoff masked by the noise of wind gusts (the vertical streaks at the lower left in the spectrogram, corresponding to the spiles in the time series at the bottom). The wind signature is strongest at low frequencies (see spectrum at left), falling off to the background at 80–200 Hz (the grey curve the power spectral density (PSD) during quiet conditions, indicating the instrument noise background level, with the purple curve showing the PSD averaged over the present observation). The helicopter blade tones are readily seen at 84 Hz and 168 Hz. Note that a continuous 195 Hz fixed tone (due to a thermal pump on the rover) has been filtered out for this spectrogram presentation. Note that the 168 Hz helicopter tone is only sporadically detectable, and the 84 Hz frequency has nonmonotonic variations in intensity. A slight waviness in the 84 Hz and 168 Hz lines is explored more closely in Fig. 10. The slight diagonal at the right is the rotor spin-down after landing.

pump that circulates liquid to convey heat from the radioisotope generator to other parts of the rover). The dominant quasi-monochromatic tones (seen as broken narrow horizontal lines in the plots) at 84 Hz and 168 Hz are due to Ingenuity. It may be recalled (e.g. Grip et al., 2022) that in powered flight, the helicopter blades rotate at a near-constant rate of 2537 rpm (42.3 Hz, i.e. half of 84 Hz), with thrust direction and magnitude controlled by changing the incidence of the blades cyclically and collectively with a swashplate i.e. like a true helicopter. It may be noted that multirotor vehicles that effect control on fixed-incidence propellers by speed changes would have rather broader and variable frequencies as the thrust to each rotor is varied. The intensity of the 84 Hz signal is seen (Fig. 6) to broadly decline and then increase again – this is largely due to the increasing then decreasing range of the vehicle, according to the flight path in Fig. 2. The 168 Hz tone similarly has a maximum received intensity when the range is minimized. We will return to some additional variations in intensity in section 3.4, see also Appendix 2.

Also notable in flight 4 is the presence of wind noise at the start of the flight – this dominates the time domain plot (Fig. 6, upper panel). Comparison with meteorological sensor data acquired during the flights suggests the corresponding wind gusts were of the order of 10 m/s (Viúdez-Moreiras et al., 2022; Maurice et al., 2022): wind noise acoustic signatures – rather broadband low-frequency noise that is quite distinct from the narrow helicopter tones - are the subject of a separate study by Stott et al. (submitted, 2022). Finally, although the rotor spin-up was obscured by a wind gust (the rotor spin-up and –down when the vehicle is on the ground are performed with the blades held at nearly zero incidences, so the aerodynamic forces (and aerodynamic noise) are relatively small, but some emission is seen at the higher speeds. The spin-down is visible from about 84 Hz to about 70 Hz on flight 4.

Flight 5 has much less wind noise, with only a couple of modest gusts (Fig. 7). The 168 Hz signal appears overall slightly fainter than before (even at the same distance – there were small differences in wind speed and direction, and in the week between flights 4 and 5, small changes in pressure and temperature meant the atmospheric density was about 3% less for the latter – e.g. Lemmon et al. (2022), so even without propagation effects the coupling efficiency from the atmosphere to microphone would have been reduced slightly). The 84 Hz signal is seen throughout the flight (although the spin-up is not noticeable) and includes a series of sharp nulls, as we discuss later.

Flight 6, starting already at some 110m distance (Fig. 4), is a much less rich record. The spin-up and a couple of cycles of 84 Hz modulation are seen before the sound fade into the background (Fig. 8) as the helicopter recedes beyond ~150m from the rover. During this flight, the 168 Hz signal is not observable even at the closest part at the beginning, due to the stronger atmospheric absorption at this frequency.

By Flight 8, the rover had caught up to the helicopter (Fig. 5) and was close enough (65m) to observe the spin-up, and about 20s of 84 Hz and 168 Hz tones before again flying out of range (Fig. 9). Acoustic recording was made during Flight 9, but at 200–500m distance, sounds were unobservable (as expected).

We may note that the directivity of the near-omnidirectional microphone is very small (e.g. Mimoun et al., 2023) and this factor cannot be responsible for the significant variations in intensity observed. At these low frequencies, the gain is constant to less than 2 dB over a 90-degree azimuth arc centered on the boresight.

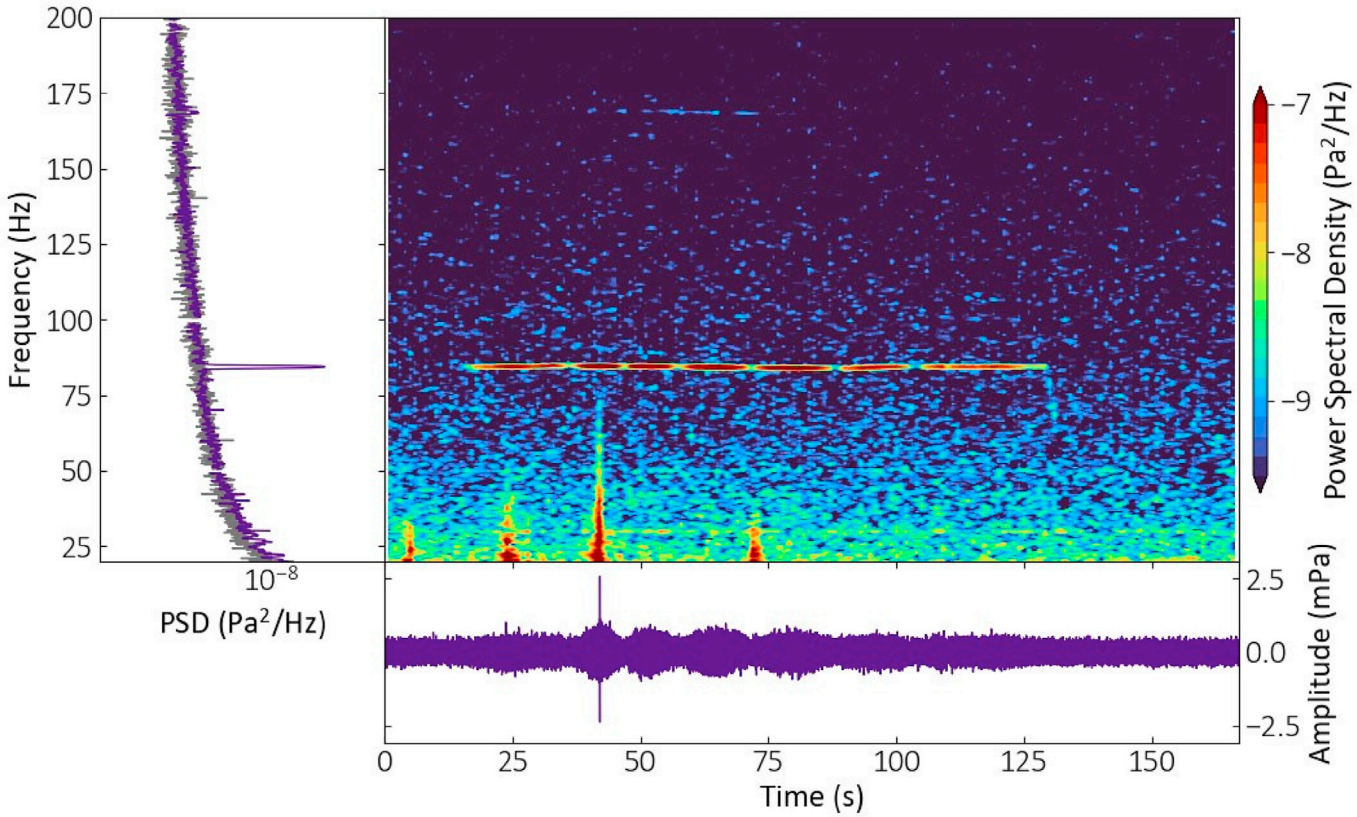

Fig. 7. The acoustic signature of flight #5 encountered relatively little wind noise. Although the helicopter trajectory is mostly a single straight line, there are increases and decreases in the received intensity of the 84 Hz tone throughout the flight. The 168 Hz tone is only barely noticeable, and for only part of the flight.

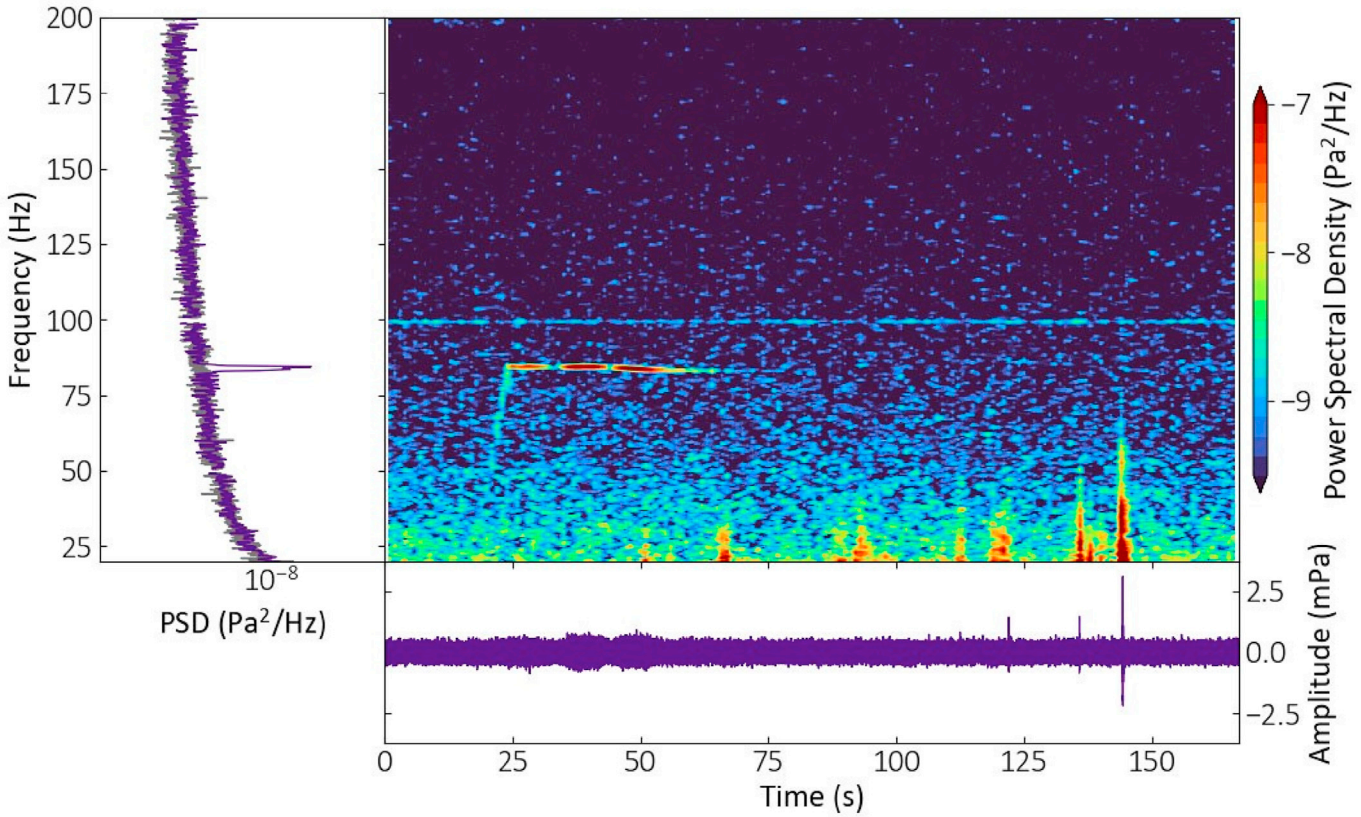

Fig. 8. Flight #6 showed for the first time the rotor spin-up, and the 84 Hz tone for part of the flight before the heli passes out of range. Unfortunately, the control anomaly occurred in the distant inaudible part of the flight. Again, only a brief signature of wind gusts is seen. A 95 Hz tone is present due to rover equipment.

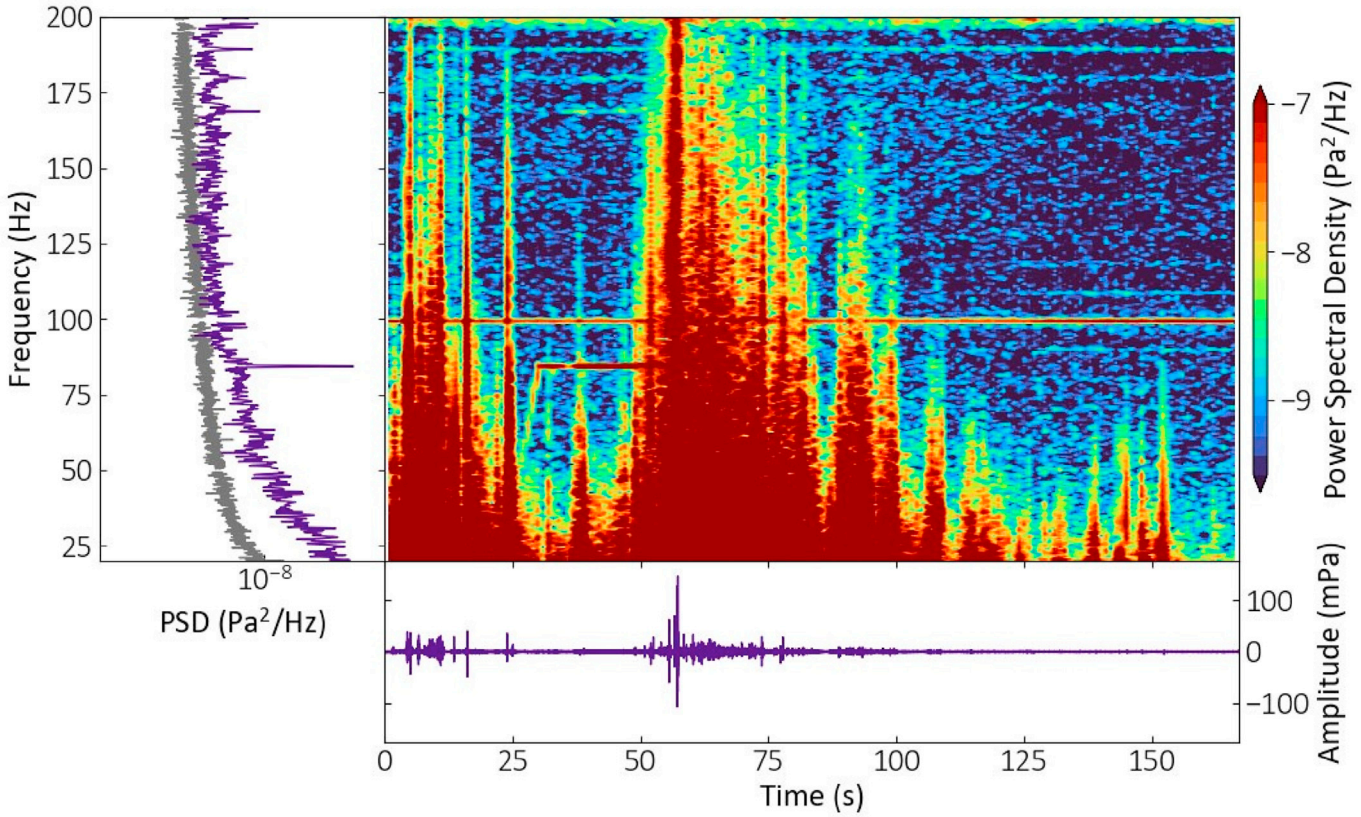

Fig. 9. Flight 8 suffered rather severe wind noise, but the rotor spin-up is observed and the 84 Hz and 168 Hz signals are observable during the first 20 s or so of the flight before the helicopter goes out of range. Horizontal lines show that rover noise is present at several frequencies: it is suspected that the signals in this instance are electromagnetic interference from the helicopter base station, near which the SuperCam mast unit was pointed during the flight.

3.2. Atmospheric attenuation of helicopter sound

The attenuation of acoustic signals by the CO_2-rich atmosphere is, as expected, much higher than that in the terrestrial atmosphere, particularly for higher frequencies. This property of carbon dioxide has been well-known since the work of Tyndall in the 1840s, and it has been noted in connection with Mars specifically by e.g. Williams (2001), Bass and Chambers (2001) and Petculescu (2016). As noted by Maurice et al. (2022), the observed attenuation is broadly consistent with these physical models: a fuller investigation of frequency dependence and model comparison is discussed elsewhere (Chide et al., submitted). Suffice it to note here that the 84 Hz principal helicopter emission was not obvious beyond ranges of about 150m on Mars, and the 168 Hz sound is observable much less than the 84 Hz. It may be also noted that a large comb of higher harmonics can be observed in terrestrial chamber tests in low-pressure CO_2 atmospheres at short distances (see Appendix 3): in these tests, the path length is short enough that the high-frequency absorption does not eliminate the sound as it does at the ~100m ranges observed on Mars.

3.3. Doppler shift of helicopter sound

Close inspection of the spectrograms (especially flight 4, Fig. 6) shows some waviness in the frequencies of the rotor tones. This is readily understood as the Doppler shift due to the helicopter flight and was most prominent in flight 4 (sol 69). There the flight speed v of 3.5 m/s was an appreciable fraction of the speed of sound (c ~243 m/s), so the Doppler shift was of the order of 84 Hz times (v/c)~1% or about 1 Hz. Because the flight was not directed towards or away from the rover, the Doppler shift was a little less than this (Fig. 10) due to the range rate being lower than the flight speed. This result shows that in principle acoustic data can yield kinematic constraints on the helicopter trajectory, if (for example) the helicopter's navigation telemetry were unavailable. The Doppler signatures in flight 5 were slightly simpler since that flight had a simpler geometry, although the lower speed meant that the peak frequency shift was only about 0.4 Hz.

3.4. Modulation of acoustic emission

The most puzzling feature of the sound recordings is the quasi-periodic modulation of the received intensity of the 84 Hz and 168 Hz tones that is not explained by the distance between the helicopter and the microphone: the most prominent example is shown in Fig. 11. Another feature of the received signatures is that the 168 Hz intensities have short-term variations that are not congruent with the 84 Hz variations–see Fig. 12. This implies a frequency-dependent feature of the emission or propagation, suggesting some sort of interference effect.

We initially speculated that these sharp nulls were caused by destructive interference from multipath propagation (a direct sound ray, and one reflected from the ground, e.g. Attenborough, 2002) – see Appendix 2. However, the fact that it was still observed while the helicopter was hovering at a fixed position does not support the sound propagation interference hypothesis. Additionally, this model (a classic problem in acoustics) proved quantitatively unable to reproduce the observed signatures with physically-realistic parameters. Measurements on a ground demonstration model of the helicopter (Appendix 4), and observations of nonsynchronous blade rotation (see next section), instead lead us to attribute the modulation to be a feature of the interaction between the two rotors on the helicopter.

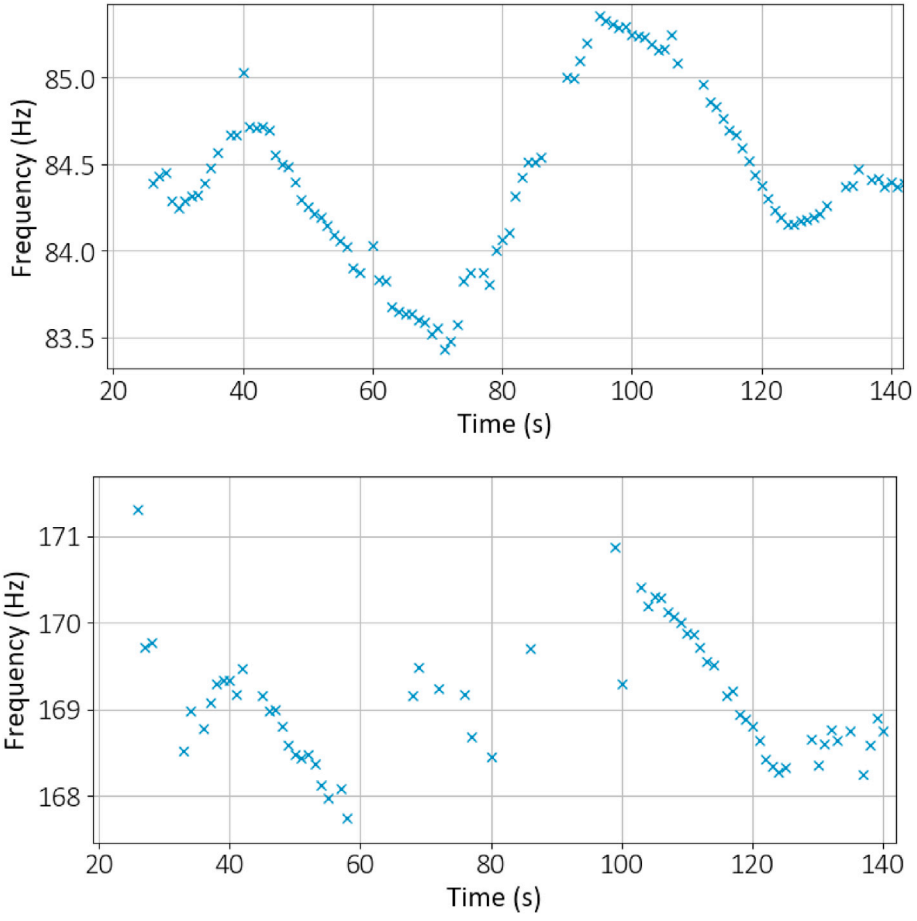

Fig. 10. Peak tonal emissions extracted from the spectrogram (Fig. 6) of flight #4 (Sol 69), showing the frequency variation. A slightly asymmetric there-and-back flight (Fig. 3) occurred along a linear path with the closest approach (zero Doppler shift) at about 50 s and 115 s. The signal is slightly blue-shifted once forward flight begins at ~35s, then progressively more and more red-shifted for 50–70 s (the flight speed is constant, but the flight direction becomes more and more parallel to the line of sight). The helicopter slows down 70–80s and reverses the flight.

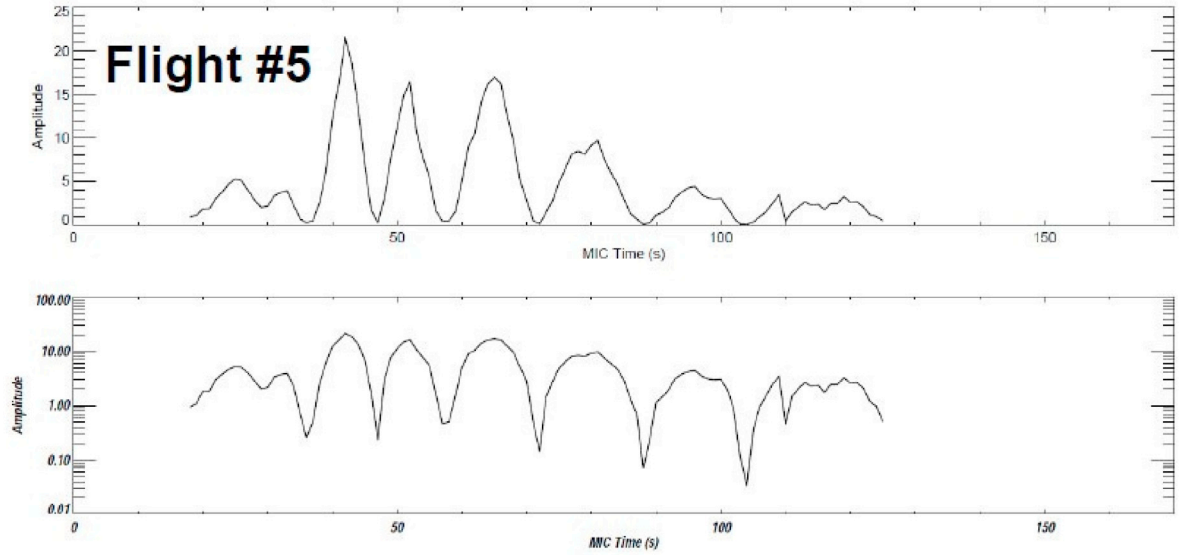

Fig. 11. Received intensity of the 84 Hz tone on flight 5 (Sol 76), shown in linear (upper) and logarithmic (lower) presentations. The overall increase in amplitude to 50s and subsequent decline is simply due to the distance, but the series of sharp nulls at 36, 47, 57, 72, 88 and 104 s cannot be explained this way.

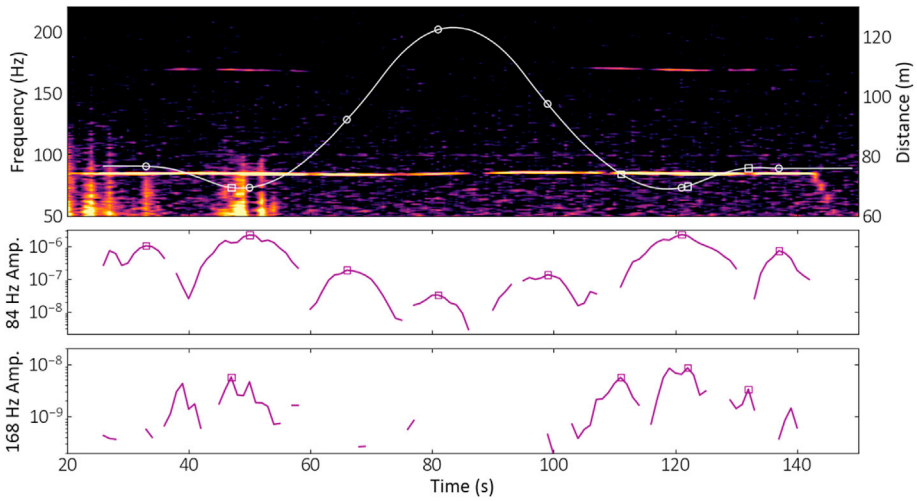

Fig. 12. The spectrogram (top panel) of flight 4 again showing that while the overall trend of the received intensity of the 84 Hz and 168 Hz tones (lower panels) is merely a reflection of distance, there is an additional effect causing modulation with a ~15s period for the 84 Hz signals. A shorter-period modulation appears on the 168 Hz signal, although since this tone is weaker overall, the record is less complete and is noisier. Of note is the null at about 90s, which appears and disappears while the helicopter is at a virtually fixed distance from the rover.

4. Mechanism of rotor sound modulation on mars

The noise from coaxial contrarotating propellers has been the subject of study for at least three quarters of a century (e.g. Hubbard, 1948; see also e.g. Hanson, 1985) but has assumed renewed importance in recent years with the proliferation of unmanned drones with such rotor arrangements in urban settings where noise is of particular concern (e.g. McKay et al., 2021). We first note some algebraic properties of superposed harmonic sources, and then discuss how the geometry and aerodynamics of the helicopter flight relate to the observed modulation. The key parameter is the Blade Passage Frequency (BPF), which is the rotation rate (Hz = rpm/60) times the number of blades on each rotor. Although the rotation rates of the upper and lower rotors are nominally the same, they are driven by separate motors and even small differences in rate lead to observable effects both acoustically and in camera data.

4.1. Algebraic superposition of sound from two monochromatic sources

We may first note that the superposition of the pressure fields from two collocated sound sources with frequencies f_1 and f_2 and equal amplitude A is linear and straightforward

$$p(t) = A\sin(2\pi f_1 t + \varphi_1) + A\sin(2\pi f_2 t + \varphi_2) \quad (1)$$

The phases φ_1,φ_2 of the two signals are for the moment arbitrary. The trigonometric sum can be re-expressed as a product of the sine of the mean of the two frequencies $f_m=(f_1+f_2)/2$ and the cosine of the half-difference of the two, $f_d= (f_1-f_2)/2$, or

$$p(t) = A\sin(2\pi f_m t + \varphi_m)\cos(2\pi f_d t + \varphi_d/2) \quad 2)$$

Again, the mean and difference phase terms φ_m, φ_d are unimportant. Since the intensity of a sound is proportional to the square of the pressure, it follows then that the intensity averaged over one or more periods (f_1~f_2) will have a modulation of $\cos^2([f_1-f_2]/2)$. This function ranges from 0 to 1 and thus can yield the deep modulation we observe, if the difference frequency is in the range 50–100 mHz (corresponding to a modulation period of 10–20s). Given the nominal rotation speed of 2537 rpm, we can associate the observed mean tone with two BPFs, e.g. f_1 = BPF_1 = 84.56 and f_2 = BPF_2 = 84.51 Hz, for example. This difference of less than 0.1% in rotor speed would have an essentially unnoticeable effect on the helicopter control:rotor forces and moments vary with the

square of rotor speed, and roughly proportionally to angle of attack of the blades (the collective control changes the blade incidence over the range −4.5° to +17°, with 10° a typical value, e.g. Lorenz, 2022). Thus a rotor speed difference of 0.1% would yield a torque difference of only~0.2%, which could be compensated for by a blade incidence angle change of only 0.02° (the accuracy of the actuators is only 0.25°) Inspection of data from the accelerometers of the helicopter's inertial measurement unit (IMU) during flight 4 show a peak at 84.4 Hz: some data segments the peak is somewhat saddle-shaped, perhaps indicating two tones separated by ~0.1%, but the data are noisy and the sample rate is only 500 Hz, rather marginal to reliably separate these frequency components.

The algebra applies equally if there are sounds produced at twice the BPF. The modulation of this tone (here, $f_1 = 2BPF_1 \sim f_2 = 2BPF_2 \sim 168Hz$) would have a modulation frequency again equal to the difference in the two frequencies. Thus the modulation period for this double-BPF (i.e. ~168 Hz) signal, $1/(2[BPF_1\text{-}BPF_2])$, is half of the modulation period of the 84 Hz signal.

4.2. A mechanistic model relating geometry to the acoustic time series

The rotors on the helicopter each spin at an essentially constant rate. Thus for there to be a modulation at all, there must be some interaction either between the rotor and the helicopter structure or between the rotors themselves. As noted previously, these questions have been confronted historically with the origination of contrarotating propellers, and with renewed vigor since the drone revolution.

The fundamental paradigm here is that a pressure disturbance is generated in the region between the rotors when they cross. For a coaxial contrarotating pair of two-bladed rotors, this pressure field is generated at 2x BPF, two times the blade passage frequency (each rotor moves through 90°). Simplistically, one can imagine the air being 'squeezed' between them – data from Torija et al. (2021) show that the intensity of the BPF_1+BPF_2 tone increases significantly relative to the BPF_1 or BPF_2 tones when the separation between the rotors is reduced from 0.1 to 0.05 rotor diameters. For illustrative purposes, we can assume that the pulse is instantaneous, and occurs only as an instantaneous point source at the tips, see Fig. 13, although we recognize that in reality there will be a complex 3-dimensional time variant pressure field, notably varying along

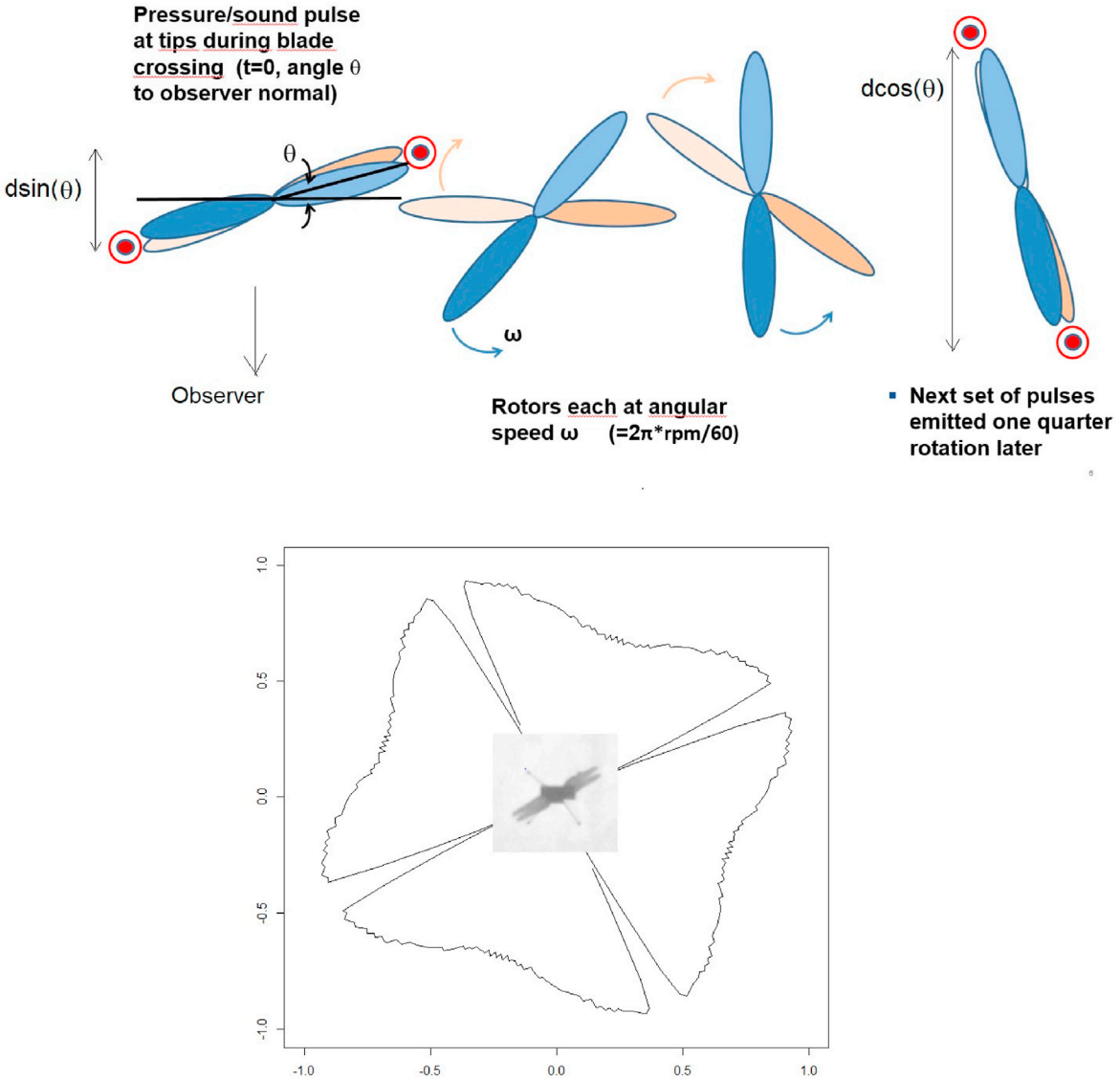

Fig. 13. 'Tip Slap' model for emission from contrarotating two-bladed rotors. 4 pressure pulses are launched every quarter rotation and their interaction yields an azimuthal sound radiation pattern with four 'lighthouse' notches parallel and orthogonal to the blade-crossing azimuth (the lower panel 'rosette' is simply the 84 Hz azimuthal emission function from Appendix 5; Fig. A8 replotted as a polar diagram.).

the span of the blade and not just at the tip (e.g. McKay et al. (2021) consider a line source).

As explained in Appendix 5, this model yields a pulse train at a distant observer with significant components in the 1x BPF and 2x BPF frequencies (in the Mars case, at 84 Hz and 168 Hz). Furthermore, these tones are modulated strongly in azimuth, such that there is a rosette-shaped (or rather, four-leaved) radiation pattern. Other frequency components are also present (at 3x, 5x BPF) and are also azimuthally varying, but on Mars, the higher harmonics are too faint to observe due to the CO_2 attenuation.

In the case of perfectly synchronous rotors, the radiation pattern would remain fixed to the helicopter. One or at most two nulls might be observed if a helicopter flew in a straight line past a fixed microphone. This is not what was seen in the Mars data. However, if the rotor speeds are very slightly different, the azimuth at which the blades cross will slowly rotate and thus the sound radiation field will also rotate like a lighthouse. An observer of a hovering helicopter will see a time series of acoustic emissions modulated at a frequency equal to the difference in rotation rates: in the case of a straight-line translating flight, there will be a modest phase variation superposed on the constant frequency difference (Fig. 14). (There is in principle an additional phase variation associated with the sound propagation time from the helicopter to the microphone, but since this is only of the order of 0.5 s, this can be neglected).

Although the rotors on the Ingenuity helicopter are driven at nominally identical speeds, they are each driven by an independent motor and small variations in rotor speeds will in any case occur as the drag on the rotors changes as the blade incidence changes in response to collective and cyclic control inputs.

An unanticipated insight into the rotor rotation speeds is yielded by the down-looking navigation camera on the helicopter. This down-looking camera is used for sequential image correlation to estimate the vehicle's horizontal velocity relative to the ground (e.g. Balaram et al., 2018; Grip et al., 2022; Lorenz, 2022). Because the flights were made near local noon, the sun was high in the sky and the navigation camera images show the shadow of the helicopter. The exposure times are sufficiently short that the rotor shadows are only slightly blurred by motion. Only a subset of navigation camera images was returned to Earth, and they stroboscopically sample the blade configuration (see Fig. 15). However, the sampling is dense enough to observe the azimuth at which the blades cross and to see (e.g. Fig. A9) that this azimuth rotates relative to the helicopter, implying that the rotors are not synchronous. Examination of the azimuth rotation of the blade crossings (which were best observed on flight 5) indicates that nulls would be observed at intervals of about 15 s, just as observed (Fig. 11).

If we consider a constant mismatch of rotor frequencies (i.e. a constant lighthouse rotation), then on flight 4, the azimuth from the helicopter to the rover will rotate anticlockwise due to the straight-line flight in one direction, and then rotate clockwise on the return leg. This azimuth change of about 70° (one-fifth of a rotation, see Fig. 2) causes a timing shift that appears consistent with the slight asymmetry in the time series of 84 Hz nulls (Fig. 12) – they are separated by about 20 s in the outbound leg, but about 24s in the return leg. On the other hand, in flight 5 with a single flight direction and thus monotonic helicopter-rover azimuth variation, the spacing between nulls slowly increases. This is broadly consistent with the pattern at which the observed blade crossings point at the rover (Fig. 16), or are orthogonal to it, namely frames A, C, E, G, J and M. Inspecting the spacecraft clock (SCLK) times associated with those images (Appendix 5) we see these are spaced at 11, 10,12, 18 and 15 s. This non-monotonic variation suggests that the assumption of a constant difference in rotation rates is not quite accurate, introducing additional degrees of freedom, so a more detailed model-fitting exercise does not appear to be justified. However, the overall consistency of these intervals with those between the acoustic nulls (see Fig. 12) of 11, 10, 15,

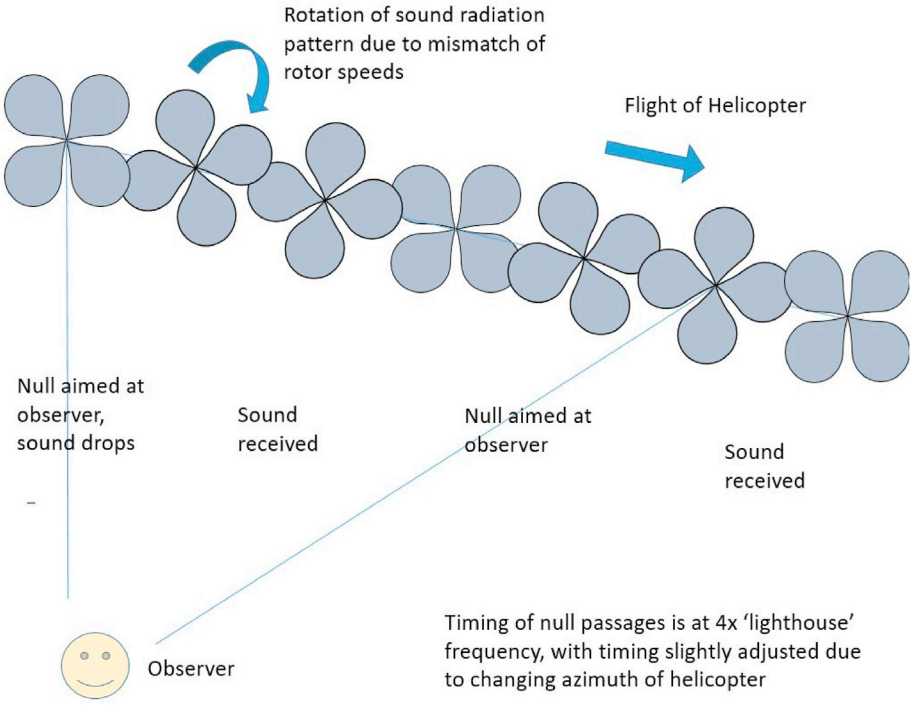

Fig. 14. Asynchronous rotors will cause a slow rotation of the four-lobed sound radiation field from the helicopter, leading to a periodic series of nulls at 4 times the difference in rotation rates. The changing azimuth of the helicopter as it flies past the observer adds a small phase difference to the observed null timing.

Fig. 15. Navigation Camera frames from flight 5, annotated with metadata from the image headers. The image numbers increment by 28, as only a subset of images were sent to Earth, and are separated by about 0.6 s. The helicopter is flying towards the left, so the scene (grey sand, with slightly darker rover tracks, and slabs of bright rock) moves towards the right, whereas the shadow of the helicopter remains fixed in the center. The shadows of the rotor blades rotate between frames: the stroboscopic snapshots occasionally show the blade crossing (bottom panel).

16 and 16 s – given that these are not determined to better than a second in any case, is a striking confirmation of the overall scenario.

5. Conclusions

A helicopter has one of the most distinctive acoustic signatures in terrestrial aviation. So it is on Mars. Recordings by the Supercam microphone on Mars 2020 have captured sounds of four flights by the Ingenuity helicopter. Wind noise is detectable in the recordings, as well as an 84 Hz blade passing frequency and occasionally its first harmonic. Higher harmonics are not observed and are believed to have been attenuated by the long (80–150m) path through the CO_2-rich atmosphere which absorbs higher frequencies. In acting as a sound source with somewhat known and constant characteristics, the combination of microphone and helicopter can be used to probe the characteristics of the Martian environment, such as the attenuation by the atmosphere.

An unanticipated feature of the recordings is a modulation with a period of the order of 10–20s. A multipath origin was investigated and rejected. Closer examination finds the behavior is reproduced by a simple model wherein a pressure pulse is launched from a line source when the rotors cross. It is an interesting coincidence that the time for a sound wave to cross the rotor disk is similar to the time for successive blade crossings for Ingenuity at Mars: this is not the case for similar rotorcraft on Earth. Looking forward to the Dragonfly octocopter mission to Titan, which may carry several microphones, this propagation effect may be important. The beating pattern of 10–20s period appears to result from a slight mismatch of the counterrotating blade rotation rates, as also shown by the changing azimuths of the blade shadows. This beating, which causes a 'lighthouse' rotating notch in the sound emission, was not observed in ground tests of the helicopter, where the microphone was mounted underneath the vehicle such that the sound had little or no azimuthal modulation.

The present paper has documented and explained most of the major features of the Ingenuity flights (although in some respects the very detection of the sound is surprising, since near-surface temperatures should bend sound rays upwards). These flights are one of the few controllable sounds audible to Perseverance, and the only source of sound detected from distances >12 m from the microphone, and are therefore critical to understanding the acoustic environment of Mars, a source of strong public interest. Furthermore, we have shown that acoustic measurements are a useful diagnostic of the rotor flight characteristics (rotor operation, and Doppler shift of the vehicle), at least to distances of ~100m, which may be relevant in supporting future Mars sample return operations involving 'fetch' helicopters (e.g. Pipenberg et al., 2022). We may note also that the Dragonfly rotorcraft lander mission to Titan, presently in development, is planned to carry one or more microphones which may serve as diagnostics of rotor/motor operation, and perhaps also to detect wind noise or other environmental sounds.

In terms of 'lessons learned', we would note that observations from much shorter distances would likely have provided more useful information on the acoustic propagation in the Martian boundary layer by permitting the detection of a wider range of emitted tones since the attenuation of these so-far unobservable frequencies would be less. Flights closer than 50m were precluded for safety reasons early in the rover mission: now that considerable experience has been acquired in helicopter operations, it may be that this policy can be re-assessed. On the other hand, other experiments can be envisaged, which would comply with the >50m safety policy – e.g. having the vehicle hover at some altitude in a fixed location might permit probing of the winds above the ground via Doppler effects. Experiments with rotor operation in a landed configuration (e.g. with low collective pitch so as not to develop much lift) could be of interest at short ranges, yielding a comb of emitted tones with a different propagation geometry from hovering flight.

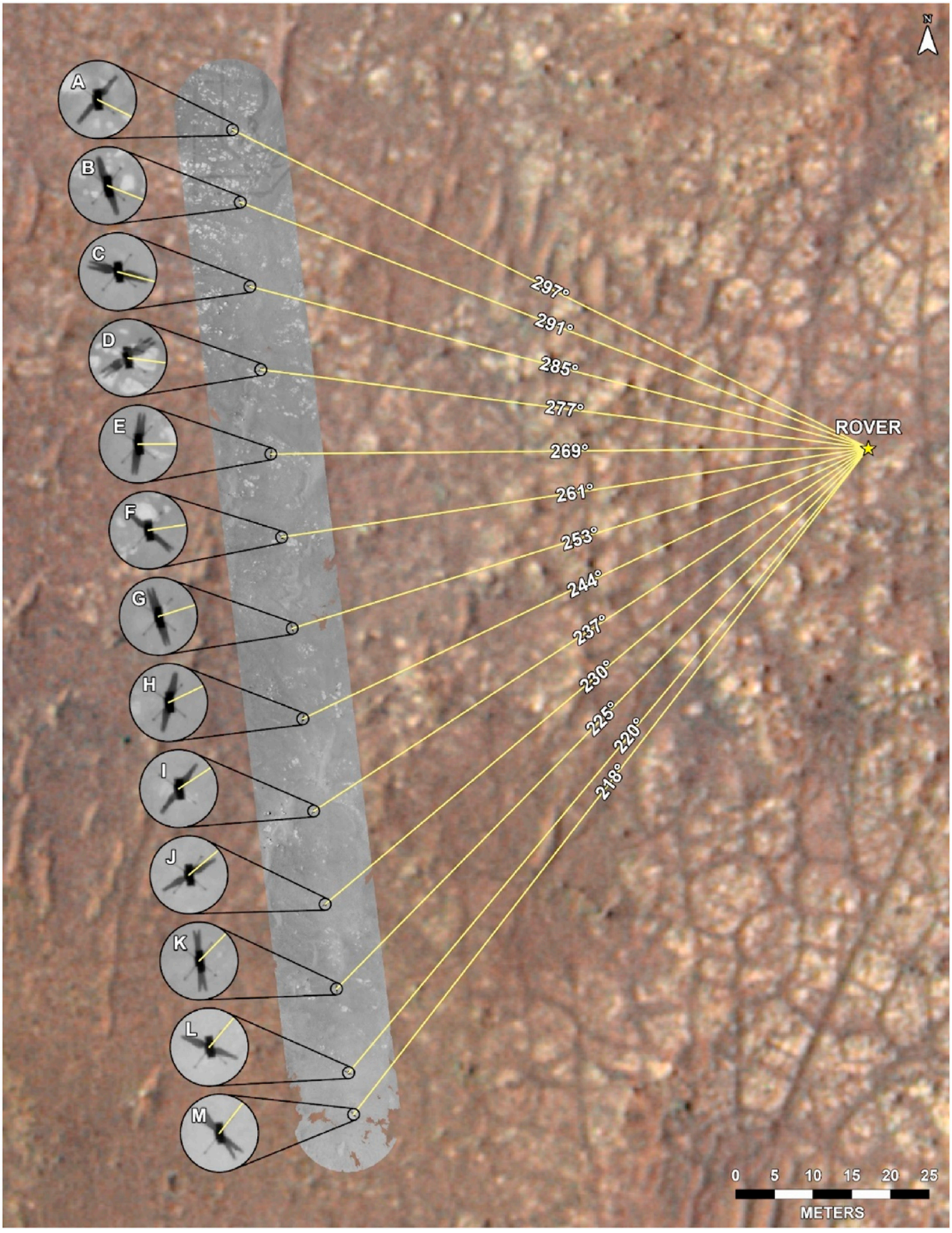

Fig. 16. A sequence of helicopter shadows in those individual navigation camera images with blade-crossings are shown overlain on a HiRISE color basemap showing the rover location. Circular enlargements adjacent to their actual location are added to show the orientation, with the yellow line indicating the vector to the rover. It is seen that the blade crossings are either parallel or orthogonal to the rover in A, C, E, G, J and M. (see Appendix 5 for image details).

Declaration of competing interest

The authors declare that they have no known competing financial interests or personal relationships that could have appeared to influence the work reported in this paper.

Data availability

Data will be made available on request.

Acknowledgements

RL is supported by the Mars 2020 Project SuperCam investigation, via contract #1655893 with the Jet Propulsion Laboratory. We thank the Mars 2020 Project for supporting acoustic observations and helicopter operations. Bart Hibbs of Aerovironment is thanked for discussion of the high frequency noise on the Terry demonstrator. Aimee Quon of JPL is thanked for confirming some details of test chamber sound recording. RCW was supported by JPL contract #1681089. B.C. is supported by the Director's Postdoctoral Fellowship from the Los Alamos National Laboratory, grant 20210960PRD3.

Appendix 1. Location and Data

Table A1
Helicopter and Rover Locations for Flights with sound recording. Coordinates are in meters. Coordinate of the farthest point on the out-and-back Flight 4 is given (and is actually very close to the Flight 5 landing point).

	Sol	Heli_Easting	Heli_Northing	Rover_Easting	Rover_Northing
Flight 4 Takeoff	69	4354501.026	1093313.230	4354573.466	1093293.855
Flight 4 Farthest *	69	4354523.031	1093179.429	4354573.466	1093293.855
Flight 4 Landing	69	4354507.059	1093313.340	4354573.466	1093293.855
Flight 5 Takeoff	76	4354507.059	1093313.340	4354589.755	1093269.989
Flight 5 Landing	76	4354522.342	1093183.397	4354589.755	1093269.989
Flight 6 Takeoff	91	4354522.342	1093183.397	4354569.045	1093272.017
Flight 6 Landing	91	4354441.082	1093123.835	4354569.045	1093272.017
Flight 8 Takeoff	120	4354452.698	1093018.168	4354410.670	1092970.249
Flight 8 Landing	120	4354488.969	1092861.839	4354410.670	1092970.249

Supercam microphone data may be obtained at the NASA Planetary Data system Perseverance archive (https://pds-geosciences.wustl.edu/missions/mars2020/). Data are in the Supercam bundle, and 'Raw' (Engineering data record – EDR) and 'Calibrated' (CDR) data volumes are available: the latter are likely most appropriate for most users. Since SuperCam's data handling system is natively set up for image data, the acoustic data are archived in Flexible Image Transport Format (FITS) files, for which readers exist in many data processing packages (e.g. R, IDL, Matlab etc.). Dedicated freeware readers also exist, e.g. fv (https://heasarc.gsfc.nasa.gov/ftools/fv/). For the convenience of acousticians and the public, raw sound records (.wav) files are also made available. The CDR data file identifiers are shown in Table A2. Note.

Table A2
Data File Identifiers

Flight	sol	cdr_fname (calibrated data)
4	69	SCAM_0069_0673066208_290_CA2_scam07069_____01P02.fits
5	76	SCAM_0076_0673687636_279_CA2_scam01076_____01P02.fits
6	91	scam_0091_0675019254_277_ca2_scam05091_heli_91_scam_mic___01p01.fits
(see note)	105	scam_0105_0676260248_420_ca2_scam05105_heli_105_scam_mic___01p01.fits
8	120	scam_0120_0677593685_336_ca2_scam06120_heli_____01p01.fits
(see note)	128	scam_0128_0678303882_432_ca2_scam05128_heli_____01p01.fits
9	133	scam_0133_0678747754_326_ca2_scam08133_heli_____01p01.fits

Note: Flight 7 was intended to be executed on Sol 105, and this Supercam microphone observation was initially planned to observe it. However, a watchdog timer anomaly on the helicopter aborted the flight which was then deferred until Sol 107 and to avoid complexity (this was the first flight after the flight 6 anomaly) and the microphone observation was not replanned. Thus flight 7 was not observed. The Sol 128 observation was similarly initially planned to observe the helicopter but no flight took place.

Table A3
Observation timing and geometry. Times shown refer to the start of the Supercam data file. Note that there is a small (tens of seconds) offset in time from the times indicated here to the start of the sound recordings, due to a mismatch between the rover clock and the Supercam clock. Attempts to correlate sound with external events or imaging should pay attention to the relevant keywords in the image header to apply the appropriate time shift. The pointing column refers to the SuperCam microphone orientation with respect to the rover forward direction (note Sol 105, for flight 8, where the microphone was pointed nearly backwards, towards the helicopter base station that may have been a strong electromagnetic noise source), whereas the azimuth columns refer to local north.

Sol	Instrument Pointing (deg)	Instrument Azimuth (deg)	Instrument Elevation (deg)	Solar Azimuth (deg)	Solar Elevation (deg)	Spacecraft Event Time (SCET)	Local Mean Solar Time	Local True Solar Time
69	110	273.0	2.7	240.4	83.7	2021-120T14:52:26.246	Sol-00069M12:35:52.033	12:22:41
76	62	218.6	0.5	251.8	83.6	2021-127T19:29:33.390	Sol-00076M12:35:58.058	12:25:12
91	351	209.7	−0.4	271.7	82.9			12:30:08

(*continued on next column*)

Table A3 (*continued*)

Sol	Instrument Pointing (deg)	Instrument Azimuth (deg)	Instrument Elevation (deg)	Solar Azimuth (deg)	Solar Elevation (deg)	Spacecraft Event Time (SCET)	Local Mean Solar Time	Local True Solar Time
						2021-143T05:23:21.888	Sol-00091M12:35:57.900	
105	194	232.2	−2.4	330.6	87.9	2021-157T14:06:45.670	Sol-00105M12:05:57.756	12:04:22
120	18	54.5	−2.1	292.7	80.5	2021-173T00:30:53.200	Sol-00120M12:35:27.941	12:38:00
128	276	98.5	−3.1	295.7	79.8	2021-181T05:47:35.868	Sol-00128M12:35:28.572	12:40:00
133	134	338.9	0.3	297.2	79.4	2021-186T09:05:31.298	Sol-00133M12:35:27.868	12:41:11

Appendix 2. Multipath models considered but rejected

In fact, motivated by experience of fading patterns in the radio signal from the Huygens probe (Pérez-Ayúcar et al., 2006) that had some similarities with the repeating nulls observed by the microphone, we considered multipath interference effects as a probable mechanism. This was not only attractive as a physically-plausible explanation of the deep modulation of the signal amplitude, but also offered the prospects of being diagnostic of the near-surface atmospheric structure and/or the acoustic reflection properties of the surface.

The simplest model (and one readily demonstrated with simple benchtop ultrasound experiments, Lorenz, 2006) is one where a direct ray of sound from the airborne helicopter to the microphone about 1.6m off the ground interferes destructively with a ray that reflects from the foreground (Fig. A1). The reflected ray has a slightly longer path, such that if the path difference approaches one half a wavelength (or N+0.5 wavelengths, with N an integer) then the signals destructively interfere and a null is observed. This was the mechanism of the Huygens multipath radio fading (and also observed on Mars with the Viking radio link). The same effect has been observed with sound on Mars (Maurice et al., 2022) in that ~6 kHz sounds received by the microphone on a short (several mm) boom ahead of the Supercam mast unit suffer interference with the sound reflected from the wall of the unit, causing a 'notch' in the received sound spectrum from broadband quasi-impulsive sounds generated by laser shots on nearby targets. The path difference, equal to ~2 cm or roughly double the boom length, corresponds to half of the sound wavelength (with speed of sound ~240 m/s, a 6 kHz signal has a wavelength of 4 cm).

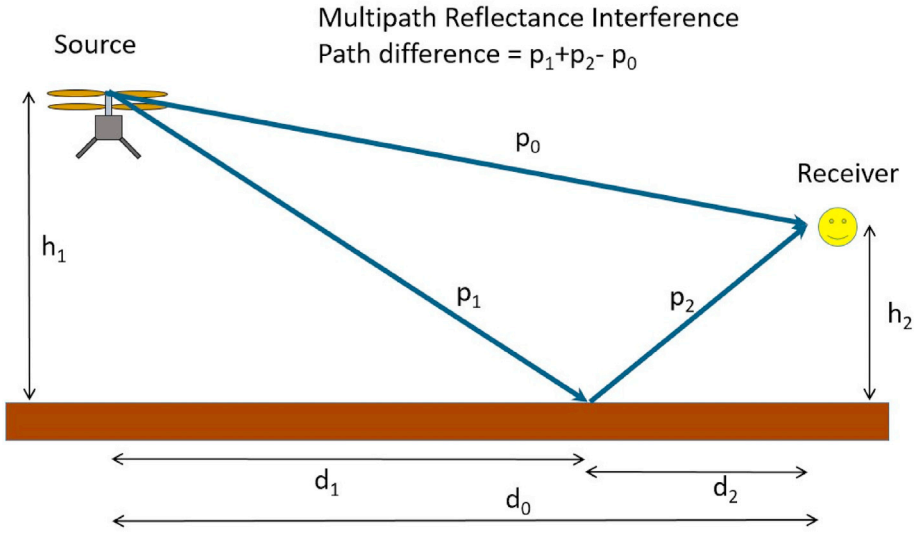

Fig. A1. Classic reflectance multipath model with interference occurring when (p1+p2-p0)=(N+0.5)λ. The same effect occurs if very strong near-surface refraction occurs to bend the ray upwards (mirage).

In this classic reflectance model (a well-studied problem in acoustics – see e.g. Norum and Liu, 1978), the position of the nulls is determined geometrically (by the lengths and their relation to the wavelength λ). The depth of the nulls depends on the angular variation of sound emission and reception, and on the reflection coefficient of the surface: for electromagnetic multipath this can be diagnostic of the surface dielectric constant and roughness, but except for very porous surfaces such as light snow, the acoustic impedance difference between the atmosphere and the surface is so strong that the reflection coefficient is close to unity and thus the null depth is not strongly constraining. The null width does depend on the scattering characteristics, being wider for a more diffuse (typically, rougher) scattering surface.

For the present problem, d0~50–100m, h1 = 5m or 10m, h2 = 1.6m and the characteristic path difference is 0.1–0.2m. This may be compared with the wavelength of the 82 Hz sound, namely 3m. Hence the phase difference range across this geometry is simply not enough to cause a set of interferences.

This purely reflective model can be elaborated by introducing a layer near the ground (from 0 to h2, say) of air with a different propagation speed. The different propagation speed in this layer causes a further phase difference between the direct and reflected ray (there is a small additional effect due to refractive bending at the interface between the slabs of atmosphere at two different temperatures). This effect is physically-plausible since steep near-surface gradients exist on Mars. In the case of a strongly-heated ground, typical of Martian daytime conditions, the near-surface can be some 20K warmer. However, model experimentation shows that these perturbations are not enough to cause the phase difference needed to generate several nulls over the flight distance.

The case of a smooth near-surface gradient is analytically more difficult, but physically even more plausible, and can lead to refractive bending near the surface such that the downgoing ray is slowly deflected back upwards. This is the acoustic equivalent of a mirage (specifically, an inferior mirage) where strongly heated air near the ground in terrestrial deserts causes upward deflection of shallow downward rays, mimicking the optical behavior of a surface mirror such as a lake. However, as before, the path difference realized by this mechanism over the ~100m distances characteristic of the helicopter flights is not enough to cause strong interference. In fact, the expected upward deflection of the sound rays by the near-surface temperature gradient actually makes it somewhat puzzling that the sound could be detected at all. More work is needed to understand this issue.

Only with a temperature inversion, such that the indirect sound ray can propagate appreciably (several to 20 m) upwards before being bent back to the ground can strong interference be developed. Such ray paths are not uncommon in the terrestrial atmosphere at night, when the near-surface atmosphere becomes chilled by radiative cooling. The optical counterpart is a superior mirage, or fata morgana, sometimes showing e.g. apparently levitated images of ships at sea that are beyond the geometric horizon. The required temperature structure is not compatible with either reasonable models nor with in-situ measurements of the Martian atmospheric conditions. Thus we are compelled to attribute the modulation of the Ingenuity acoustic signals to time-varying emission, rather than effects of the propagation path.

Appendix 3. Audio Characteristics of Ingenuity Mars Chamber Tests

Flight tests of various development units (Fig. A3) of the Mars helicopter were conducted in Mars-like atmospheres in the 85-ft space simulation chamber at JPL (see e.g. Lorenz, 2022). Various development configurations of the helicopter were flown (for example, with different spacing between the rotors; a 'Phase 3' vehicle flew with rotor speed of 2600 rpm, whereas an Engineering Development Model (EDM) was flown predominantly at 2277 rpm, thus the sound frequencies differ slightly.) In many such tests (e.g. https://vimeo.com/431875747) audio recordings were made, in part for outreach. The microphone was placed on a test stand support, close to and typically a meter or two below the hovering helicopter.

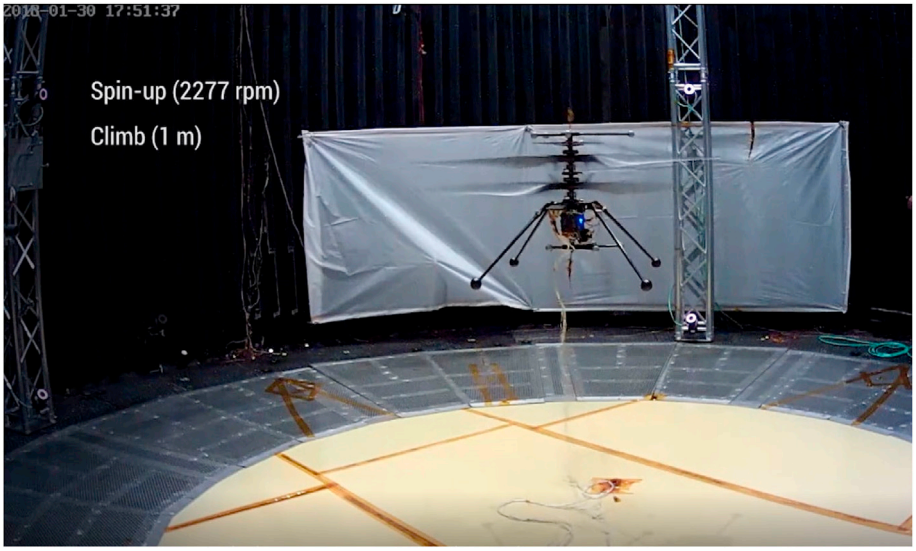

Fig. A2. Hover test in chamber at Mars pressure.

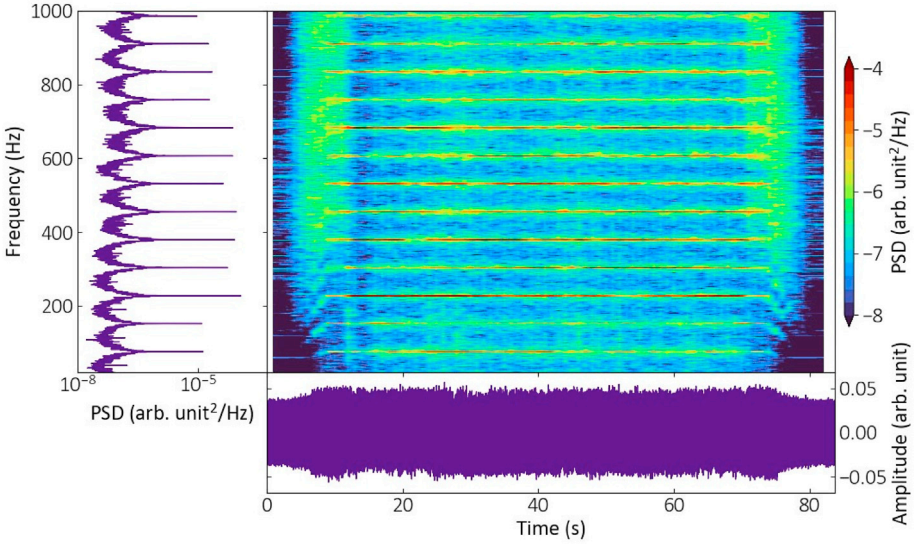

Fig. A3. Spectrum/spectrogram and time series of hover test in Mars chamber. Note the striking series of harmonics of the 82 Hz signal. Spin-up and spin-down can be noticed at the start and end of the record.

It is seen (Fig. A3) that there is a wide comb of emitted frequencies, at multiples of the blade passage frequency. This is typical of contrarotating propellers (e.g. Torija et al., 2021; McKay et al., 2021; Hanson, 1985). We might expect to see such a comb on Mars if the Ingenuity helicopter were permitted to hover above or near the Perseverance rover: however, this was precluded for operational safety reasons and at the longer distances at which acoustic observations of flights were made, the higher harmonics have been attenuated by atmospheric absorption such that they could not be observed.

By comparing Supercam microphone recordings of the background noise in the test chamber with the outreach video sound recorded in the chamber just prior to the helicopter flight, we estimate the sound pressure level of the helicopter flight to be about 0.05 Pa.

There is some modulation of the intensity of the different harmonics in the test: some of this is likely due to movement of the helicopter within the chamber, such that different path lengths, different off-boresight gains of the microphone, and/or different echo interference, resulted. We have not attempted to interpret these variations.

Appendix 4. Observations of terrestrial demonstrator helicopter "Terry"

Motivated by the observations on Mars, some measurements were made on an aerodynamically-similar demonstration helicopter, referred informally by its constructors at Aerovironment, Inc. as "Terry". This article uses exactly the same rotor configuration as Ingenuity on Mars. The article is slightly less massive (1.44 kg vs 1.8 kg) than Ingenuity, although in their respective gravity environments, Terry weighs about double (14N vs 6.7N). However, in the terrestrial sea level atmosphere, with a density about 50 times higher than Mars (e.g. Lorenz, 2022), the required rotor speed to achieve hover thrust to balance this weight is much less – about 400 rpm vs 2537 rpm on Mars. The Terry unit, intended principally for demonstration purposes, is radio-controlled by a human operator (rather than by autonomous autopilot as at Mars) and the motor speed control electronics is quite different. While the Mach and Reynolds number of the rotor flows are somewhat different, the identical rotor geometry would be informative regarding acoustic emission. A variety of acoustic and pressure/infrasound measurements were made with the helicopter in free (indoor) flight, or secured to the laboratory floor (see Fig. A4).

Because the flights had to take place indoors, acoustic reflections precluded any attempt to replicate the rotating sound field of the Mars model. Furthermore, the flight controls did not permit independent variation of the two rotor spin rates. However, microphones placed on the ground beneath Terry did show that a peak in local intensity was synchronized with blade passage. The far-field acoustic emission spectrum (Fig. A5) showed characteristic peaks at the blade passage frequency of 14 Hz and its overtone at 29 Hz, as well as an intermediate frequency of 21 Hz. A variety of acoustic (and possibly electrical) interferences such as air handling in the building likely contribute to many of the emission peaks. The broad 900 Hz emission appears to be obviously associated with the helicopter and may be related to magnetostrictive noise associated with the 24 pairs of magnets on each motor (which is a 3-phase motor) yielding ~918 Hz.

Since the 4 rotor blades (2 on each rotor) have an area of approximately 0.05 m^2, and the typical suction peak on an airfoil is about 4x the average, it follows that the peak pressure excursion associated with an individual rotor blade (or its tip vortex) on Terry may be of the order of 14/.05–280 Pa. When the vehicle was in hover about 1m above an infrasound sensor on the ground, pressure fluctuations of the order of 5 Pa were observed.

Fig. A4. Demonstration helicopter "Terry" secured to the laboratory floor by weighted bags. The investigator is holding a flashlight that illuminates two photodiode sensors underneath the rotor blades so that readings from pressure and acoustic sensors could be synchronized with blade passage via the shadow signals. The investigator is masked per Aerovironment policy at this stage of the Covid pandemic (September 2021).

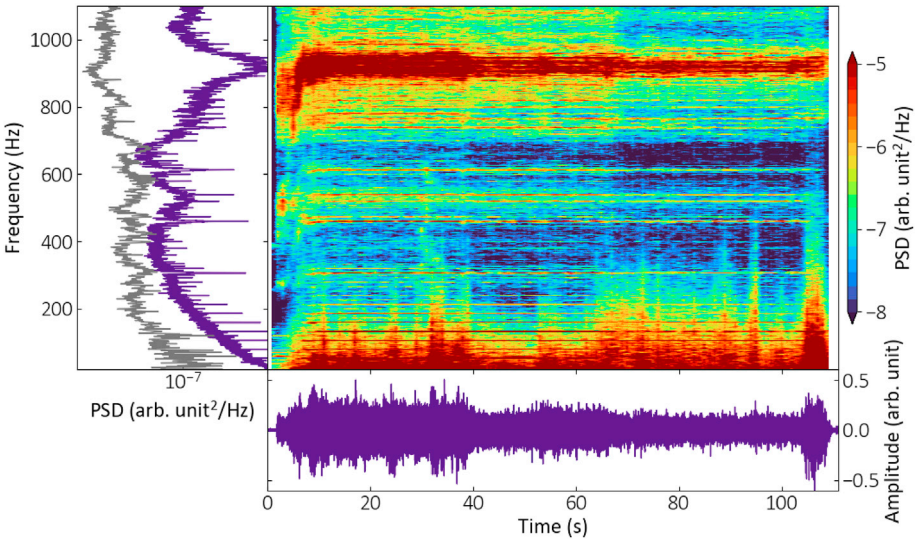

Fig. A5. Spectrogram of the acoustic emission from Terry in tethered ground test (three collective settings, from ~10 to 40s, from 40s to ~65s, and from 65s to 105s). No attempt has been made to account for the frequency response of the sound recorder (TEAC-10, stated to have 3 dB response down to 20 Hz) but it is seen that prominent peaks exist at 14, 21 and 29 Hz. Note the broad emission around 900 Hz, whose source is not known. It may be noted that the 21 Hz signal is relatively prominent – its counterpart on Mars at 126 Hz was not seen.

Appendix 5. Idealized Acoustic Emission Model

As described in the text, pressure pulses are launched from the blade tips at 2x the BPF. However, the phase of their arrival at a distant observer depends on the blade azimuth, and on the time for a pulse to propagate across the rotor disk.

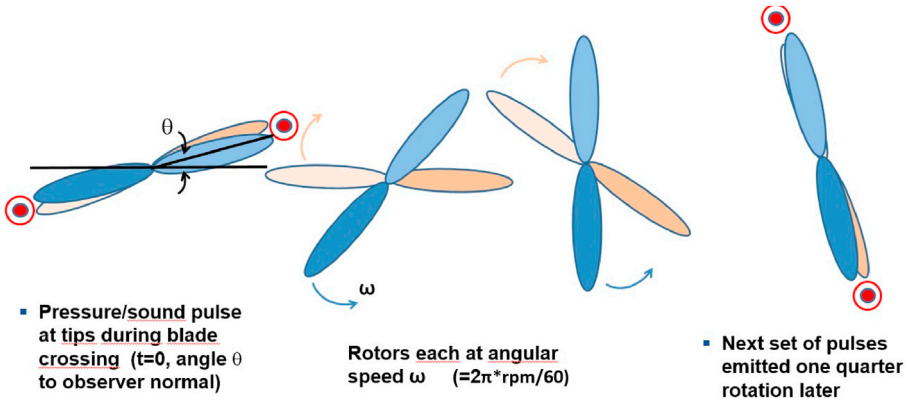

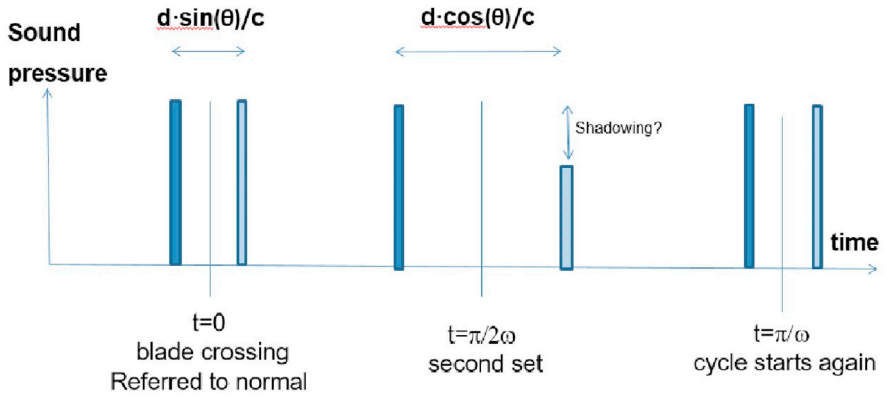

Fig. A6. Heuristic model of blade-slap emission model. A distant observer can detect two pairs of pressure pulses per blade passage interval (twice the rotor rotation rate): depending on the ratio of rotation period to the propagation time across the disk, these pairs may collapse, influencing the relative intensity of the 2x and 4x BPF frequencies.

A timescale of interest is D/c, the time it takes a pressure wave to propagate from one side of the rotor disk to the other, with D the rotor diameter (1.2m) and c the speed of sound. On Earth (c~340 m/s), this timescale is about 3.5 ms, whereas on Mars (c~250 m/s) it is about 4.8 ms. Then, a distant observer at an azimuth θ from the normal to the blade crossing will hear these two pulses a time Dcos(θ)/c apart.

Since, for two-bladed rotors, another blade crossing occurs one quarter of a rotation later, another pair of pulses is launched an interval π/2ω after the first, or 0.5/BPF. This pair will arrive at the observer spaced by Dsin(θ)/c.

The spectral character of the sound will depend on the ratio of these two timescales. In the case of a very small rotor diameter, D/c is small compared with π/2ω and the pulses from the two tips are heard almost instantaneously, with little rotational modulation. The close doublet pulses are heard at twice the blade passage frequency, i.e.at π/2ω. In the case where D/c is comparable with π/2ω, however, the doublets are appreciably split when the blade crossing is not orthogonal to the observer. An example of the observed pulse train and resultant frequency spectrum is shown in Fig. A7, and the azimuthal variation in emission is shown in Fig. A8.

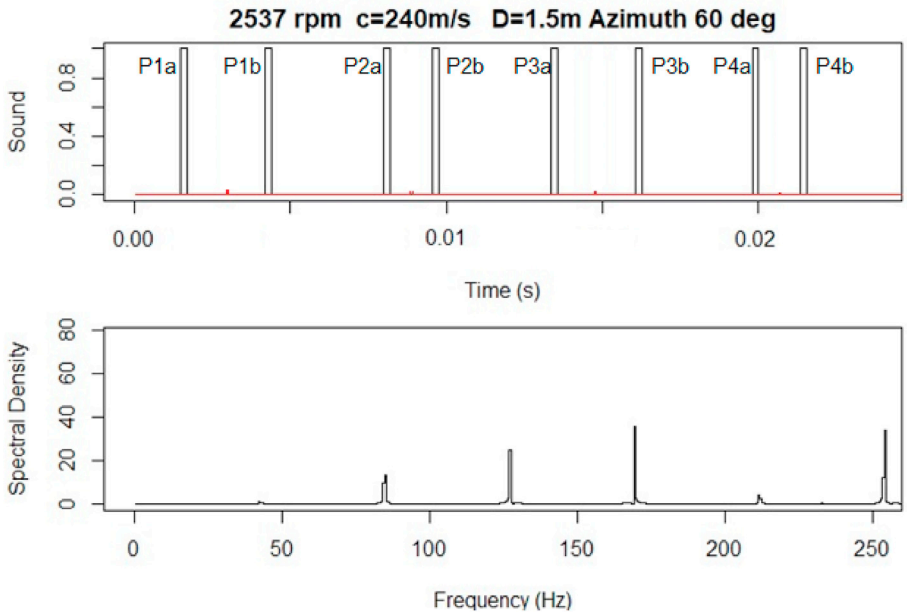

Fig. A7. (Upper panel) Time series of sound pulses received in the far field from one rotor revolution (23.6ms, at 2537 rpm) In one revolution the blades cross four times, producing a pair of pressure pulses each time. The pulses are produced at the same instant, but reach a distant observer separated by an interval that depends on theta. (Lower panel) Emitted spectrum for this idealized 'tip slap' model for parameters representative of Mars and a blade crossing azimuth theta of 60°. Tones are present at 84 Hz and 168 Hz, as well as higher harmonics (likely attenuated away at Mars). A deficiency of the model is that it also predicts some emission at 126 Hz, which was not observed. The relative intensities of the different harmonics depends on θ, and on the actual pressure pulse shape (shown in upper panel only as a notional square wave).

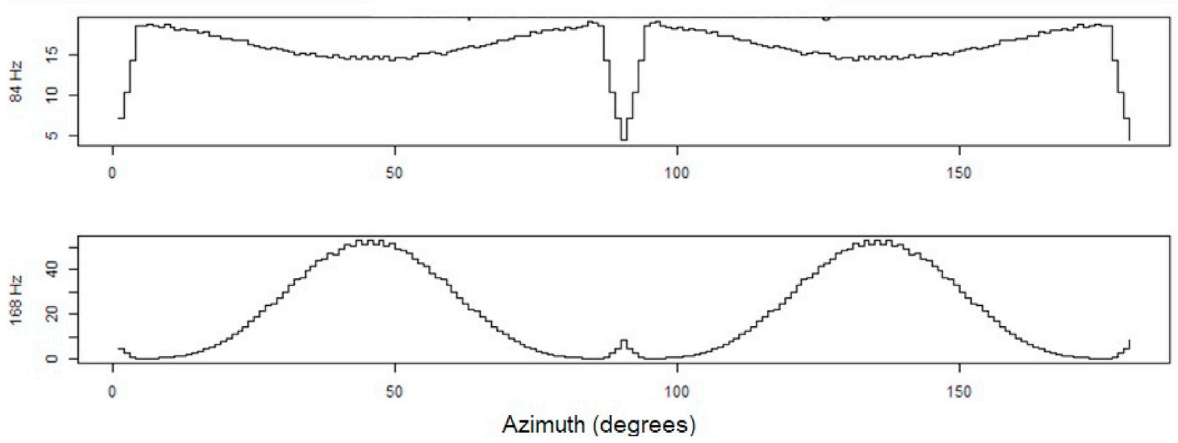

Fig. A8. Sound intensity at 1x and 2x BPF as a function of azimuth. The 84Hz signal has a sharp null near zero and ninety degrees, whereas the 168 Hz frequency in this model instantiation has a quasisinusoidal characteristic.

This model, while simple, was inspired by the measurements taken in Appendix 4 and appears to capture the main features of the sound observed on Mars, influence by the blade asynchrony evident e.g. in. Clearly, the model could be elaborated by the convolution of the impulses at the moment of crossing with more general waveforms corresponding to the pressure field along and between the rotor blades as a function of the angular separation. A further elaboration might be that the distant pressure pulse might be blocked by the helicopter body for some small range of angles around the anti-observer direction. A full investigation of the model parameter space is beyond the scope of this paper, however.

The navigation camera images used in Fig. 16 are as follows.

A) HNM_0076_0673687483_278FDR_N0050001HELI00848_0000LUJ02
B) HNM_0076_0673687488_652FDR_N0050001HELI01010_0000LUJ02
C) HNM_0076_0673687494_026FDR_N0050001HELI01172_0000LUJ02
D) HNM_0076_0673687499_400FDR_N0050001HELI01334_0000LUJ02
E) HNM_0076_0673687504_780FDR_N0050001HELI01496_0000LUJ02
F) HNM_0076_0673687510_148FDR_N0050001HELI01658_0000LUJ02
G) HNM_0076_0673687516_119FDR_N0050001HELI01838_0000LUJ02
H) HNM_0076_0673687522_095FDR_N0050001HELI02018_0000LUJ02
I) HNM_0076_0673687528_062FDR_N0050001HELI02198_0000LUJ02
J) HNM_0076_0673687534_033FDR_N0050001HELI02378_0000LUJ02
K) HNM_0076_0673687539_407FDR_N0050001HELI02540_0000LUJ02
L) HNM_0076_0673687544_781FDR_N0050001HELI02702_0000LUJ02
M) HNM_0076_0673687549_558FDR_N0050001HELI02846_0000LUJ02

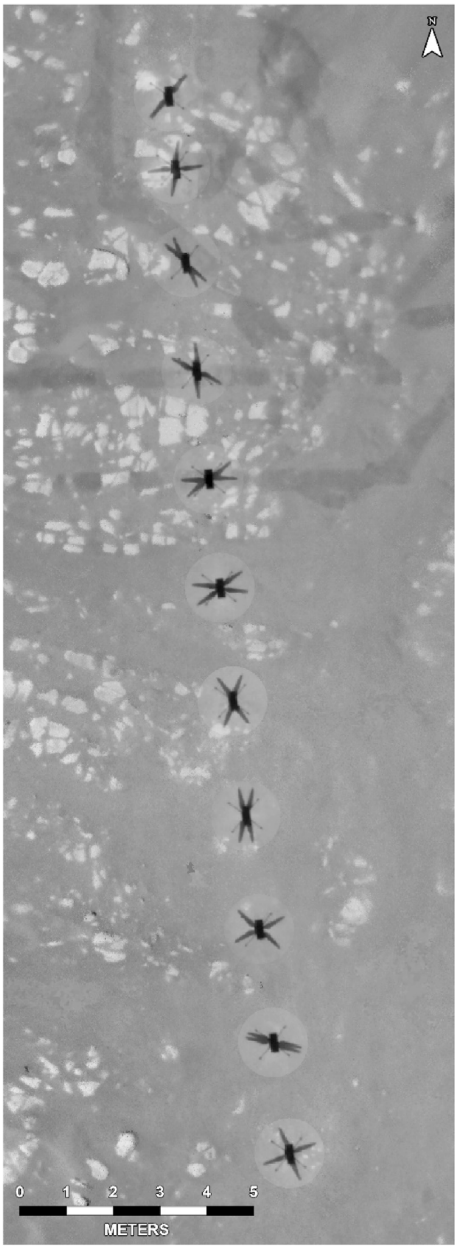

Fig. A9. The navigation camera images from flight 5 have been co-registered to make an orthomosaic: this forms the grey strip in Fig. 16. Then the circular image segments (1.5m diameter) showing helicopter shadows from every other downlinked frame from 848 to 1208 have been superposed in their corresponding locations. The rotation of the blade-crossing azimuth is evident.

References

Attenborough, K., 2002. Sound propagation close to the ground. Annu. Rev. Fluid Mech. 34 (1), 51–82. https://doi.org/10.1146/annurev.fluid.34.081701.143541, 2002.

Bell III, J.F., Maki, J.N., Alwmark, S., Ehlmann, B.L., Fagents, S.A., Grotzinger, J.P., Gupta, S., Hayes, A., Herkenhoff, K.E., Horgan, B.H., Johnson, J.R., 2022. Geological, multispectral, and meteorological imaging results from the Mars 2020 Perseverance rover in Jezero crater. Sci. Adv. 8 (47), eabo4856.

Chide, B., Bertrand, T., Lorenz, R., Munguira, A., Hueso, R., Sanchez-Lavega, A., Martinez, G., Spiga, A., Jacob, X., de la Torre Juarez, M., Lemmon, M., Banfield, D., Newman, C.E., Murdoch, N., Stott, A., Mimoun, D., Viúdez-Moreiras, D., Pla-Garcia, J., Larmat, C., Lanza, N.L., Rodríguez Manfredi, J.A., Wiens, R.C., 2023. Large and rapid air temperature fluctuations near Mars' surface revealed by acoustic measurements onboard Perseverance. Geophys. Res. Lett. 49. https://doi.org/10.1029/2022GL100333.

Chide, B., X. Jacob, A. Petculescu, R. Lorenz, S. Maurice, F. Seel; Susanne Schröder; Roger C. Wiens; Martin Gillier, N Murdoch, N. L. Lanza, T. Bertrand, P. Pilleri, D. Mimoun, M. de la Torre Juarez, R. Hueso, A. Munguira, A. Sánchez-Lavega, G. Martinez, C. Larmat, J. Lasue, C. Newman, J. Pla-Garcia, P. Bernardi, A.-M. Harri, M. Genzer, A. Lepinette, Measurements of sound propagation in Mars' lower atmosphere, Earth Planet Sci. Lett., (submitted).

Grip, H.F., Conway, D., Lam, J., Williams, N., Golombek, M.P., Brockers, R., Mischna, M., Cacan, M.R., 2022. Flying a helicopter on Mars: how ingenuity's flights were planned, executed, and analyzed. Montana. In: 2022 IEEE Aerospace Conference, *Big Sky*, pp. 5–12. https://doi.org/10.1109/AERO53065.2022.9843813. March 2022.

Hanson, D.B., 1985. Noise of counter-rotation propellers. J. Aircraft 22 (7), 609–617.

Hubbard, H.H., 1948. Sound from Dual-Rotating and Multiple Single-Rotating Propellers, NACA TN 1654. National Advisory Committee on Aeronautics, Washington, DC. July 1948.

Ingård, U., 1953. A review of the influence of meteorological conditions on sound propagation. J. Acoust. Soc. Am. 25 (3), 405–411.

Lemmon, M.T., Lorenz, R.D., Rabinovitch, J., Newman, C.E., Williams, N., Sullivan, R., Golombek, M.P., Bell III, J.F., Maki, J.N., Vicente-Retortillo, A., 2022. Lifting and transport of Martian dust by the Ingenuity helicopter rotor downwash as observed by high-speed imaging from the Perseverance rover. J. Geophys. Res. Planets 127. https://doi.org/10.1029/2022JE007605.

Lorenz, R.D., 2006. Demonstrations of multipath interferences. SERVO 4 (5), 35–38. May 2006.

Lorenz, R.D., 2022. Planetary Exploration with Ingenuity and Dragonfly : Rotary-Wing Flight on Mars and Titan, 978-1-62410-636-1, vol. 194. American Institute of Aeronautics and Astronautics. June 2022.

Maurice, S., Wiens, R.C., Bernardi, P., Caïs, P., Robinson, S., Nelson, T., Gasnault, O., Reess, J.-M., Deleuze, M., Rull, F., Manrique, J.-A., Abbaki, S., Anderson, R.B., André, Y., Angel, S.M., Arana, G., attault, T., Beck, P., Benzerara, K., Bernard, S., Berthias, J.-P., Beyssac, O., Bonafous, M., Bousquet, B., Boutillier, M., Cadu, A., Castro, K., Chapron, F., Chide, B., Clark, K., Clavé, E., Clegg, S., Cloutis, E., Collin, C., Cordoba, E.C., Cousin, A., Dameury, J.-C., D'Anna, W., Daydou, Y., Debus, A., Deflores, L., Dehouck, E., Delapp, D., De Los Santos, G., Donny, C., Doressoundiram, A., Dromart, G., Dubois, B., Dufour, A., Dupieux, M., Egan, M., Ervin, J., Fabre, C., Fau, A., Fischer, W., Forni, O., Fouchet, T., Frydenvang, J., Gauffre, S., Gauthier, M., Gharakanian, V., Gilard, O., Gontijo, I., Gonzalez, R., Granena, D., Grotzinger, J., Hassen-Khodja, R., Heim, M., Hello, Y., Hervet, G., Humeau, O., Jacob, X., Jacquinod, S., Johnson, J.R., Kouach, D., Lacombe, G., Lanza, N., Lapauw, L., Laserna, J., Lasue, J., Le Deit, L., Le Mouélic, S., Le Comte, E., Lee, Q.-M., Legett IV, C., Leveille, R., Lewin, E., Leyrat, C., Lopez-Reyes, G., Lorenz, R., Lucero, B., Madariaga, J.M., Madsen, S., Madsen, M., Mangold, N., Manni, F., Mariscal, J.-F., Martinez-Frias, J., Mathieu, K., Mathon, R., McCabe, K.P., McConnochie, T., McLennan, S.M., Mekki, J., Melikechi, N., Meslin, P.-Y., Micheau, Y., Michel, Y., Michel, J.M., Mimoun, D., Misra, A., Montagnac, G., Montaron, C., Montmessin, F., Moros, J., Mousset, V., Morizet, Y., Murdoch, N., Newell, R.T., Newsom, H., Nguyen Tuong, N., Ollila, A.M., Orttner, G., Oudda, L., Pares, L., Parisot, J., Parot, Y., Pérez, R., Pheav, D., Picot, L., Pilleri, P., Pilorget, C., Pinet, P., Pont, G., Poulet, F., Quantin-Nataf, C., Quertier, B., Rambaud, D., Rapin, W., Romano, P., Roucayrol, L., Royer, C., Ruellan, M., Sandoval, B.F., Sautter, V., Schoppers, M.J., Schröder, S., Seran, H.-C., Sharma, S.K., Sobron, P., Sodki, M., Sournac, A., Sridhar, V., Standarovsky, D., Storms, S., Striebig, N., Tatat, M., Toplis, M., Torre-Fdez, I., Toulemont, N., Velasco, C., Veneranda, M., Venhaus, D., Virmontois, C., Viso, M., Willis, P., Wong, K.W., 2021. The SuperCam instrument suite on the Mars 2020 rover: Science objectives and Mast-Unit description. Space Sci. Rev. 217 (3), 1–108.

Maurice, S., Chide, B., Murdoch, N., Lorenz, R.D., Mimoun3, D., Wiens, R.C., Stott, A., Jacob, X., Bertrand, T., Montmessin, F., Lanza, N.L., Alvarez-Llamas, C., Angel, S.M., Aung, M., Balaram, J., Beyssac, O., Cousin, A., Delory12, G., Forni, O., Fouchet, T., Gasnault, O., Grip, H., Hecht, M., Hoffman, J., Laserna, J., Lasue, J., Maki, J., McClean, J., Meslin1, P.Y., Le Mouélic, S., Munguira, A., Newman, C.E., Rodríguez Manfredi, J.A., Moros, J., Ollila, A., Pilleri, P., Schröder, S., de la Torre Juárez, M., Tzanetos, T., Stack, K.M., Farley, K., Williford, K., and the SuperCam team, 2022. In situ recordings of Mars soundscape. Nature 605, 653–658. https://doi.org/10.1038/s41586-022-04679-0.

McKay, R.S., Kingan, M.J., Go, S.T., Jung, R., 2021. Experimental and analytical investigation of contra-rotating multi-rotor UAV propeller noise. Appl. Acoust. 177, 107850.

Mimoun, D., Cadu, A., Murdoch, N., Chide, B., Sournac, A., Parot, Y., Bernardi, P., Pilleri, P., Stott, A., Giller, M., Shridar, V., Maurice, S., Wiens, R., the SuperCam Team, 2023. The Mars microphone onboard SuperCam. Space Sci. Rev. 219, 5. https://doi.org/10.1007/s11214-022-00945-9, 2023.

Newman, C.E., Hueso, R., Lemmon, M.T., Munguira, A., Vicente-Retortillo, Á., Apestigue, V., Martínez, G.M., Toledo, D., Sullivan, R., Herkenhoff, K.E., Juárez, M., Richardson, M.I., Stott, A.E., Murdoch, N., Sanchez-Lavega, A., Wolff, M.J., Arruego, I., Sebastián, E., Navarro, S., Gómez-Elvira, J., Tamppari, L., Viúdez-Moreiras, D., Harri, A.-M., Genzer, M., Hieta, M., Lorenz, R.D., Conrad, P., Gómez, F., McConnochie, T.H., Mimoun, D., Tate, C., Bertrand, T., Bell III, J.F., Maki, J.N., Rodriguez-Manfredi, J.A., Wiens, R.C., Chide, B., Maurice, S., Zorzano, M.-P., Mora, L., Baker, M.M., Banfield, D., Pla-Garcia, J., Beyssac, O., Brown, A., Clark, B., Lepinette, A., Montmessin, F., Fischer, E., Patel, P., del Río-Gaztelurrutia, T., Fouchet, T., Francis, R., Guzewich, S.D., 2022. The dynamic atmospheric and aeolian environment of Jezero crater, Mars. Sci. Adv. 8 eabn3783. https://www.science.org/doi/10.1126/sciadv.abn3783.

Norum, T.D., Liu, C.H., 1978. Point source moving above a finite impedance reflecting plane— experiment and theory. J. Acoust. Soc. Am. 63 (4), 1069–1073. https://doi.org/10.1121/1.381839 avr.

Pérez-Ayúcar, M., Lorenz, R., Floury, N., Prieto-Cerdeira, R., Lebreton, J.-P., 2006. Bistatic observations of Titan's surface with the Huygens probe radio signal. J. Geophys. Res.: Planets 111, E07001. https://doi.org/10.1029/2005JE002613.

Petculescu, A., 2016. Acoustic properties in the low and middle atmospheres of Mars and Venus. J. Acoust. Soc. Am. 140 (2), 1439–1446.

Piercy, J.E., Embleton, T.F., Sutherland, L.C., 1977. Review of noise propagation in the atmosphere. J. Acoust. Soc. Am. 61 (6), 1403–1418.

Pipenberg, B.T., Langberg, S.A., Tyler, J.D., Keennon, M.T., 2022. Conceptual design of a Mars rotorcraft for future sample fetch missions. In: 2022 IEEE Aerospace Conference, Big Sky, Montana, 5-12 March 2022. https://doi.org/10.1109/AERO53065.2022.9843820.

Stott, A. E. N. Murdoch, M. Gillier, D. Mimoun, D. Banfield, A. Chavez, B. Chide, M. de la Torre Juarez, R. Hueso, R. Lorenz, G. Martinez, Amunguira, L. M. Sotomayor, S. Navarro, C. Newman, P. Pilleri, J. PlaGarcia, J. Antonio Rodriguez-Manfredi, A. Sanchez-Lavega, D Viudez Moreiras, N. Williams, S. Maurice, R C. Wiens, Wind and turbulence observations with the microphone on Perseverance, submitted https://www.essoar.org/doi/10.1002/essoar.10512263.1.

Torija, A.J., Chaitanya, P., Li, Z., 2021. Psychoacoustic analysis of contra-rotating propeller noise for unmanned aerial vehicles. J. Acoust. Soc. Am. 149 (2), 835–846.

Tzanetos, T., Aung, M., Balaram, J., Grip, H.F., Karras, J.T., Canham, T.K., Kubiak, G., Anderson, J., Merewether, G., Starch, M., Pauken, M., 2022. Montana. In: Ingenuity Mars Helicopter: From Technology Demonstration to Extraterrestrial Scout. In 2022 IEEE Aerospace Conference, *Big Sky*, pp. 5–12. https://doi.org/10.1109/AERO53065.2022.9843428. March 2022.

Viúdez-Moreiras, D., Lemmon, M., Newman, C.E., Guzewich, S., Mischna, M., Gómez Elvira, J., Sánchez-Lavega, A., Herkenhoff, K., de la Torre, M., Rodríguez-Manfredi, J.A., Lorenz, R.D., Navarro, S., Pla-García, J., Hueso, R., Richardson, M., Smith, M., Apéstigue, V., Toledo, D., Bell, J., 2022. Winds at the Mars 2020 landing site. Part 1: near-surface wind patterns at Jezero crater. J. Geophys. Res. 127. https://doi.org/10.1029/2022JE007522.

Williams, J.P., 2001. Acoustic environment of the Martian surface. J. Geophys. Res.: Planets 106 (E3), 5033–5041.